Recent advances in transition metal sulfide-based electrocatalysts and photocatalysts for nitrogen fixation

Tarekegn Heliso Dolla [a,*], Thabo Matthews [b], Nobanathi Wendy Maxakato [b], Patrick Ndungu [c], Tiziano Montini [d,*]

[a] Department of Chemistry, Wolaita Sodo University, P.O.Box 138, Wolaita Sodo, Ethiopia
[b] Department of Chemical Sciences, University of Johannesburg, Doornfontein 2028, Johannesburg, South Africa
[c] Department of Chemistry, University of Pretoria, 0001 Pretoria, South Africa
[d] Department of Chemical and Pharmaceutical Sciences, INSTM Trieste Research Unit and ICCOM-CNR Trieste Unit, University of Trieste, via L. Giorgieri 1, 34127 Trieste, Italy

ARTICLE INFO

Keywords:
Photocatalysts
Electrocatalysts
Nitrogen fixation
Metal sulfides
Efficiency
Active sites

ABSTRACT

Ammonia production through electrocatalytic and photocatalytic N_2 fixation approaches has attracted a huge interest as a sustainable and clean route owing to the use of renewable energy to drive the processes. However, these approaches do not fulfil the industrial requirement because of the poor catalytic activity and efficiency of the catalysts. Therefore, rationally designed and highly efficient catalysts are urgently needed. Transition metal sulfide-based catalysts have gained great research interest as promising materials to catalyze artificial ammonia synthesis due to their structural similarity to the active site of the natural nitrogenase. This review gives some insights into the recent progress on the developments of transition metal sulfide-based electrocatalysts and photocatalysts for nitrogen fixation to ammonia under ambient conditions. A prospect on the future development on the rational design of efficient metal sulfide-based catalysts for artificial N_2 fixation is also discussed.

* Corresponding authors.
E-mail addresses: tarekegn.heliso@wsu.edu.et (T. Heliso Dolla), tmontini@units.it (T. Montini).

1. Introduction

Nitrogen is a vital building block for amino acids, nucleotides and other important biological compounds in plants and animals [1,2]. Earth's atmosphere is mainly composed of nitrogen in the form of molecular nitrogen (N_2), constituting around 78 % by volume. But, nitrogen molecules cannot be directly utilized by most organisms and thus need to be converted into ammonia or nitrate [3]. Therefore, the fixation of nitrogen to ammonia is one of the most vital chemical process in nature, made possible by diazotrophic organisms that contain the nitrogenase enzyme [4]. The nitrogenase catalyzes the fixation of nitrogen to ammonia by utilizing redox-active FeMo-cofactor (Fig. 1) in cooperation with reductase enzyme. The nitrogenase commonly consists of two independent proteins, a charge-transfer Fe protein and N_2-fixing MoFe protein, both containing metal-sulfur clusters [5,6]. During reaction, electrons delivered from the reductase are transferred to the Fe protein and eventually to the FeMo cofactor (FeMoco), where the conversion of N_2 to NH_3 occurs [7]. The electrons get accumulated at the MoFe protein for the reduction of N_2 into two NH_3 molecules along with the reductive elimination of one H_2 molecule (eq (1)) [8,9].

$$N_2 + 8H^+ + 16MgATP + 8e^- \rightarrow 2NH_3 + H_2 + 16MgADP + 16P_i \quad (1)$$

Ammonia is essential for industrial chemical synthesis, playing a key role as a main component for commercial chemicals like fertilizers and fibers [11,12]. It may also be used in fuel cells because of its suitability as a hydrogen energy carrier in its liquid form and is under consideration as fuels for ships and planes to replace fossil fuels [13,14]. NH_3 is most commonly produced in industry through the Haber-Bosch process, which is carried out at high temperature (400–500 °C) and pressure (15–25 MPa) [15]. This process involves a gas-phase reaction between N_2 and H_2 molecules using Fe or Ru-based catalysts (equation 2) [16]. Due to the high temperature

$$N_2(g) + 3H_2(g) \rightarrow 2NH_3(g)\,\Delta H_{298K} = -92.2\ kJ\ mol^{-1} \quad (2)$$

and pressure conditions, it is highly energy-consuming and releases large amount of CO_2 contributing to the global greenhouse gas emissions [17]. Apart from this, the hydrogen is conventionally generated through an energy intensive steam methane reforming process. Thus, to reduce CO_2 emissions and minimize energy input during the fixation process, exploration of alternative nitrogen fixation processes, which can operate under milder conditions and based on sustainable technologies, is of considerable significance.

In recent years, several alternative processes have been examined for a sustainable NH_3 synthesis under mild conditions [18] such as photocatalysis [19], electrocatalysis [20], thermal/solar-thermal catalysis [21], and plasma catalysis [22,23]. Among which, photocatalysis and electrocatalysis have gained huge research interest among scientists [24]. Photocatalytic nitrogen reduction offers a green NH_3 production path owing to the abundant and clean solar energy and the earth abundant H_2O reductant used in this process [24,25]. Electrochemical N_2 reduction is another attractive alternative due to the availability of electrical energy produced by photovoltaic plants, inducing an intensive research activity in the development of efficient electrocatalysts [20,26,27]. But these processes display very low efficiency and thus still need efficient catalysts to break the strong N≡N bond. Therefore, designing excellent catalysts to boost the electrocatalytic and photocatalytic nitrogen fixation efficiencies is highly demanded.

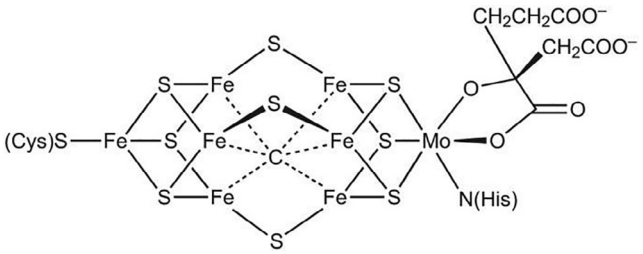

Fig. 1. Structure of the FeMo-co of the Mo-nitrogenase [10].

Inspired by nature, transition metal sulfides are considered as promising materials to catalyze artificial ammonia synthesis on their surface due to their structural similarity to the active site of the nitrogenase [17,18]. The metal-sulfur bonds in the nitrogenase enzyme are believed to help in retaining low-valence charge density sites on the metal [28] that facilitate the N_2 adsorption and subsequent polarization and activation [29]. Metal sulfides have recently attracted a widespread research interest as photocatalysts and electrocatalysts for nitrogen fixation due to their distinctive structural features, rich active sites, adjustable electronic properties and relatively narrow bandgaps [30–36].

Herein, the review elucidates the recent advances on the developments of transition metal sulfide-based electrocatalysts and photocatalysts for N_2 fixation to NH_3. After a brief introduction of the fundamental principles of the NRR, the different kinds of metal sulfides and their composites reported recently for photocatalytic and electrocatalytic NRR is systematically summarized. The focus of this review is to explain the strategies to enhance the NRR activity of transition metal sulfides including modification with co-catalysts, interfacial and defect engineering, crystal phase engineering, modulating morphology, and constructing heterostructures. Finally, we present a brief summary, prospects on the state-of-the-art transition metal sulfide-based catalysts, main challenges, and future perspectives in this research field.

2. Fundamentals of nitrogen fixation

Nitrogen fixation is a process, where gaseous nitrogen (N_2) is converted into useful chemicals such as NH_3, NO_3^-, and NO_2^- by combining with other elements and using energy input. It is a multielectron process and involves N_2 adsorption, activation and breaking of the N≡N bond, hydrogenation of N_2, and ammonia desorption. A sustained elec-

Table 1
Hydrogenation reactions and the corresponding reduction potential vs RHE during nitrogen fixations [25].

Reactions	E^o (V)
$H_2O \rightarrow 1/2O_2 + 2H^+ + 2e^-$	1.23
$2H^+ + 2e^- \rightarrow H_2$	0
$N_2 + e^- \rightarrow N_2^-$	−4.16
$N_2 + H^+ + e^- \rightarrow N_2H$	−3.2
$N_2 + 2H^+ + 2e^- \rightarrow N_2H_2$	−1.10
$N_2 + 4H^+ + 4e^- \rightarrow N_2H_4$	−0.36
$N_2 + 5H^+ + 4e^- \rightarrow N_2H_5^+$	−0.23
$N_2 + 6H^+ + 6e^- \rightarrow 2NH_3$	0.55
$N_2 + 8H^+ + 8e^- \rightarrow 2NH_4^+$	0.27

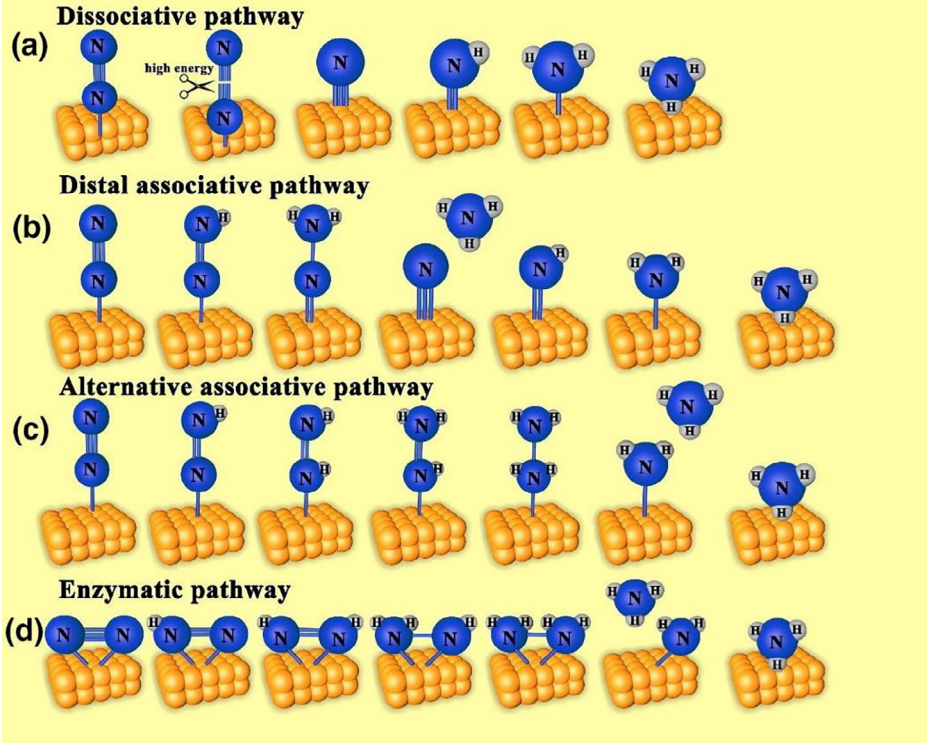

Fig. 2. The conventionally accepted mechanisms for reduction of nitrogen to ammonia. Reproduced with permission from [38]. Copyright 2021, Elsevier.

tron supply is the key to this process, which can highly support a continuous N_2 fixation reaction. The N≡N bond activation to form N_2^- on the surface of catalysts is the rate-limiting step due to its high activation energy and high reduction potential (-4.16 V vs RHE) (Table 1) [37].

Currently, there are three well known mechanisms for the catalytic nitrogen fixation to ammonia; the dissociative, associative and enzymatic mechanism [38]. The dissociative mechanism proceeds by cleavage of N≡N bond first, and then NH_3 gradually forms via hydrogenation. Typically, the well-known Haber-Bosch process is believed to undergo through the dissociative mechanism (Fig. 2(a)). In the associative mechanism, there are two possible pathways; distal and alternating pathways, referring to the different intermediates [39]. As shown in Fig. 2, in the distal pathway, the single N atom furthest away from the surface is preferentially hydrogenated releasing the first one equivalent of NH_3. Then the remaining nitride-N is hydrogenated. Whereas, in the alternating pathway, hydrogenation takes place on each of the two nitrogen atoms alternately until one of the nitrogen is converted into NH_3 and the N—N bond is broken. Different from the above-mentioned pathways, enzymatic mechanism (Fig. 2 (d)) undergoes by adsorbing the nitrogen molecule on the catalysts by the edge of each atom rather than one side and the hydrogenation occurs to both the N atoms at the same time. It usually occurs with nitrogenases and some catalysts.

2.1. Photocatalytic nitrogen fixation

As an environmentally friendly and energy-saving process, photocatalytic nitrogen fixation directly produces NH_3 from sunlight, N_2, and H_2O. Since the earliest investigation by Schrauzer and Guth [40] on titania based nanostructured materials, many catalytic materials have been explored to enhance the photocatalytic performance and improve NH_3 yield. However, the conversion efficiency is still low as a result of the recombination of electron-hole pairs and limited active sites.

The overall photocatalytic nitrogen fixation involves three key steps (Fig. 3) [41,42]. The first step is photoexcitation, in which the semiconductor absorbs solar energy generating photoelectrons. These photogenerated electrons are excited to the conduction band (CB) while holes are created and retained in the valence band (VB). Then the photoelectrons and holes are transferred to the active site on the surface of the photocatalyst to drive reduction and oxidation reactions, respectively. In the last step, the adsorbed N_2 molecules are reduced to yield ammonia by the photogenerated electrons as shown in equation (3). The H_2O or other sacrificial reagents are oxidized by the photogenerated holes to generate H^+, O_2, CO_2 and other by products. Equa-

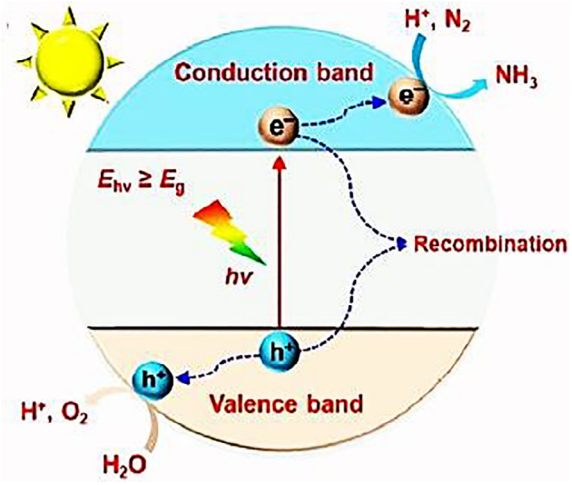

Fig. 3. A Schematic diagram of photo-driven nitrogen fixation using semiconductor photocatalysts in an aqueous solution. Reproduced with permission [43]. Copyright 2021, Springer Nature.

tion (5) shows the overall process of photocatalytic NH_3 synthesis from N_2 and H_2O under ambient conditions.

$$6H^+ + N_2 + 6e^- \rightarrow 2NH_3 \quad (3)$$

$$2H_2O + 4H^+ \rightarrow 4H^+ + O_2 \quad (4)$$

$$2N_2 + 6H_2O \rightarrow 4NH_3 + 3O_2 \quad (5)$$

2.2. Electrocatalytic nitrogen reduction

Electrocatalytic nitrogen reduction is highly considered as a promising and ecofriendly technology to achieve N_2 fixation to produce NH_3 and has attracted wide attention [27]. As the cost of electricity derived from renewable sources continues to decrease, this route can provide an alternative pathway to the energy intensive Haber-Bosch process and has the advantage of scalability. Electrochemical nitrogen reduction is a multistep process involving a proton-coupled 6-electron reduction process and produces two ammonia molecules per dinitrogen molecule. The electrocatalytic NRR process encompasses the following elementary steps: 1) diffusion of N_2 into the surface; 2) activation of N_2 molecules to intermediates via the participation of protons and multiple electron transfer; and 3) desorption of the reduced product from the surface. In the concrete process, the water oxidation and N_2 reduction occur in the anode and cathode, respectively, in a three-electrode system. The corresponding reactions in acidic and basic media are shown as follows:

Acidic condition

Anode

$$3H_2O \rightarrow 3/2O_2 + 9H^+ + 6e^- \quad (6)$$

Cathode

$$6H^+ + 6e^- + N_2 \rightarrow 2NH_3 \quad (7)$$

Alkaline condition

Anode

$$6OH^- \rightarrow 3/2O_2 + 3H_2O + 6e^- \quad (8)$$

Cathode

$$6H_2O + N_2 + 6e^- \rightarrow 2NH_3 + 6OH^- \quad (9)$$

Overall reaction

$$N_2 + 3H_2O \rightarrow 3/2O_2 + 2NH_3 \quad (10)$$

3. Recent advances in metal sulfide-based photocatalysts

3.1. CdS-based materials

CdS is demonstrated as a very attractive visible light driven photocatalyst with a strong broad light absorption owing to its narrow band gap (2.4 eV) and appropriate band structure [44–46]. However, it easily oxidizes under light irradiation and suffers photocorrosion, limiting its applications [47,48]. Various strategies were employed to improve the activity and stability of CdS including formation of solid solutions, modification with co-catalysts, and metal atom doping.

Dong et al. investigated $Zn_{1-x}Cd_xS$ (x = 0, 0.2, 0.4, 0.6, 0.8, 1) solid solution photocatalysts with a twin structure composed of major zinc blende and minor wurtzite phases [49]. Among the $Zn_{1-x}Cd_xS$ solid solutions, the $Zn_{0.8}Cd_{0.2}S$ (x = 0.2) achieved an optimal photocatalytic NH_3 yield rate of 66.91 μmol $g^{-1}h^{-1}$ under visible light and an apparent quantum efficiency (AQE) of 3.77 % at 420 nm. This NH_3 production rate is much greater compared to the ones from the pristine CdS and ZnS. The significantly enhanced photocatalytic N_2 fixation of the $Zn_{0.8}Cd_{0.2}S$ solid solution can be accounted for enhanced electron-hole pair separation by the inner homojunctions formed between the two crystal phases.

The main challenge in the photocatalytic nitrogen reduction is the low activity and low efficiency of the semiconductors because of the fast electron-hole pairs recombination. Modifying semiconductors with cocatalysts helps to tackle this challenge by enhancing charge separation and providing abundant active sites for N_2 activation. Ye and coworkers designed a Ni_2P cocatalyst loaded $Cd_{0.5}Zn_{0.5}S$ solid solution photocatalyst [50]. An ammonia production rate of 254 μmol $g_{cat}^{-1}h^{-1}$ was achieved on the $Ni_2P/Cd_{0.5}Zn_{0.5}S$ under visible light illumination without using any scavengers. A high quantum efficiency of 4.32 % was attained at 420 nm. The NH_3 yield rate is 35.7 times more than that of $Cd_{0.5}Zn_{0.5}S$ implying the role of Ni_2P cocatalyst in promoting transfer of photogenerated electrons and holes and enhancing stability. In another study, Shen and coworkers developed a metal-free cocatalyst of black phosphorous nanosheets (BPNS) to improve the nitrogen fixation activity of CdS photocatalyst [51]. They prepared the BPNS by a scalable electrochemical expansion method from bulk black phosphorus (BP) with large surface area and it provides good support for the growth of CdS nanoparticles. The BPNS/CdS composite with the optimal BPNS content of 1.5 % achieved NH_3 production rate of 240.17 μmol $g^{-1}h^{-1}$ under visible light illumination and employing methanol as the sacrificial reagent. This photocatalytic activity of BPNS/CdS is 3.69 times more than that of bare CdS, demonstrating the key role of BPNS in accelerating the charge separation and transfer.

Another study done by Gao et al. demonstrated the fascinating aspect of cocatalysts in promoting N_2 adsorption [32]. Employing NiS as a cocatalyst on CdS, N_2 molecules were observed to adsorb favorably onto the surface of NiS/CdS and is evidently displayed in the temperature programmed desorption (TPD) profiles (Fig. 4(d)). The composite exhibited excellent N_2 fixation capability of 2.8 and 1.7 mg L^{-1} in 1 h under full spectrum and visible light, respectively (Fig. 4 (a&b)). With increasing NiS loading from 0.1 wt% to 1.0 wt %, the ammonia production rate was shown to increase 1.7 times reaching 1.7 mg $L^{-1}h^{-1}$ (Fig. 4(b)). This enhancement in activity is ascribed to the improved N_2 adsorption and better charge separation efficiency brought about by the NiS loaded on CdS. Recently, a hybrid material composed of oxygen-doped 1T-MoS_2 nanosheets with rich sulfur vacancy (SV) loaded on CdS nanorods displaying an exceptional photocatalytic performance has been reported [52]. The CdS loaded with 30 wt% sulfur vacant 1T-MoS_2 cocatalysts displayed an outstanding photocatalytic ammonia production rate of 8220.83 μmol/Lh^{-1} g^{-1} under simulated solar light (Fig. 5). Compared to CdS/ (0.1 wt %) Pt, the ammonia production rate of SV-1T-MoS_2/CdS is increased by 2.36 times, exceeding Pt as a co-catalyst. This photocatalytic activity is one of the best among the previously reported non-noble metal-based photocatalysts. The metallic 1T phase MoS_2 with rich sulfur vacancies has more exposed active edge sites. The presence of the sulfur vacancy defects in SV-1T-MoS_2 is confirmed by XPS analysis as shown in Fig. 5(e) & (f), which indicates the shifts in the corresponding peak of Mo 3d positions and the difference in proportion of 1T phase in SV-1T-MoS_2 and 1T-MoS_2 samples. Thus, the SV-1T-MoS_2 offers a superior performance to SV-1T-MoS_2/CdS composite by promoting N_2 adsorption, enhancing light absorption and facilitating efficient charge separation and transfer.

Introducing defects by creating vacancies on the surface of photocatalysts has recently been realized to promote nitrogen activation and protonation [53,54]. Specifically, for transition metal-based photocatalysts such as metal sulfides anion vacancies help in constructing more active sites. By making use of the vacant d orbitals, the transition metal accepts electron density from the nitrogen p-orbital, forming a σ bond. This is followed by a back donation of the electron density from the d orbital of TM to the π* of N_2, eventually weakening the N—N triple bond. Hu and his colleagues constructed a series of ternary metal sulfides by heterometal doping to introduce surface sulfur vacancies

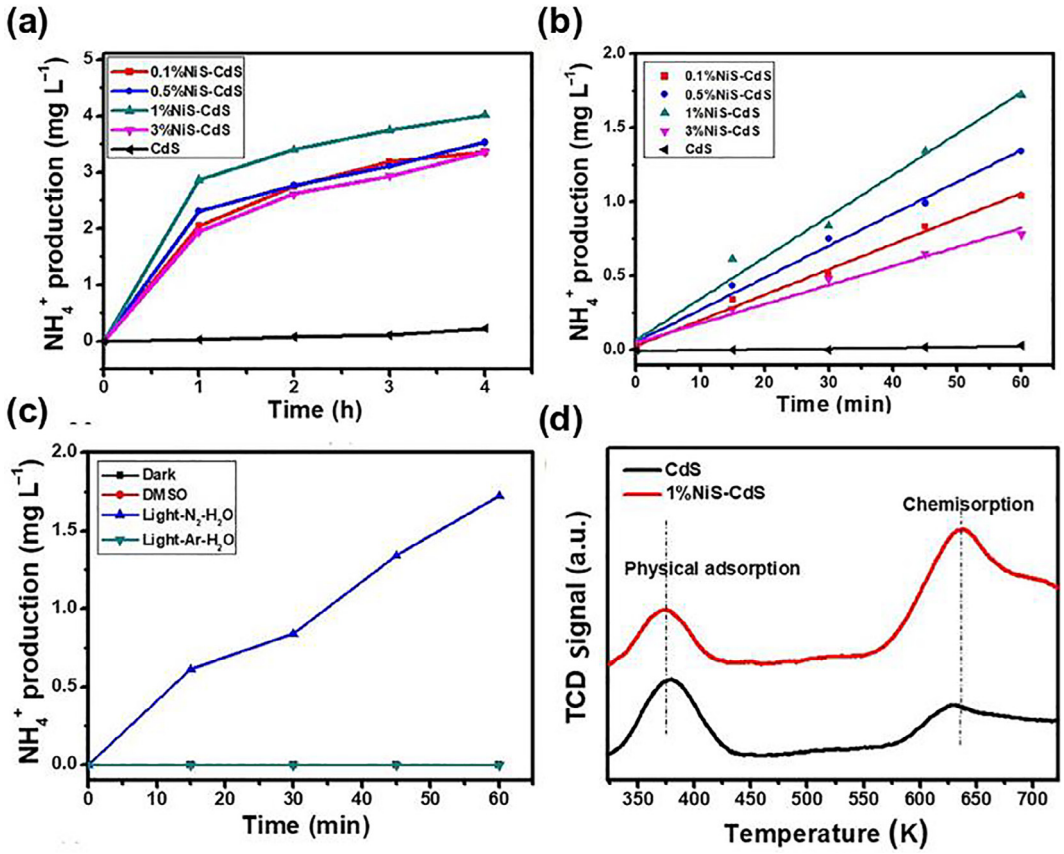

Fig. 4. (a) NH_4^+ production changes with the reaction time under full spectrum light irradiation. (b) NH_4^+ production changes with the reaction time under the visible light irradiation ($\lambda > 420$ nm) within 1 h. (c) NH_4^+ production under different conditions (darkness, DMSO as solvent and water + light + N_2 or Ar) and exposure to visible light. (d) Temperature programmed desorption (TPD) curves of N_2 on CdS and NiS/CdS. Reproduced with permission from [32]. Copyright 2019, Elsevier.

on CdS [55,56]. They synthesized the ternary metal sulfides $Zn_{0.1}Sn_{0.1}Cd_{0.8}S$, $Zn_{0.1}Mo_{0.1}Cd_{0.8}S$, $Ni_{0.1}Sn_{0.1}Cd_{0.8}S$, and $Mo_{0.1}Ni_{0.1}Cd_{0.8}S$ by using Ni, Sn, Mo, and Zn dopants. The metal doping causes the crystal lattice distortions as shown in the XRD patterns in Fig. 6(c) and induces the formation of surface sulfur vacancies, which acts as active sites for N_2 binding. Moreover, the EPR spectra given in Fig. 6(d) further confirms the formation of sulfur vacancies. They demonstrated that there is a direct relationship between the photocatalytic N_2 fixation activity and sulfur vacancy concentration (Fig. 6(a) & (b)). The sulfur vacancies were shown to be tuned by controlling the type and proportion of the metal cations.

3.2. 2D MS_2 (M = Mo, W)-based materials

2D Transition-metal dichalcogenides (TMDC) such as MoS_2, $MoSe_2$, $MoTe_2$, WS_2, and WSe_2 have drawn extensive research interest in catalysis due to their high activity, chemical stability and tunable electronic properties [57,58]. Recently, Li and coworkers have theoretically elucidated that 2D transition-metal disulfides can be considered as highly promising materials for an efficient N_2 fixation with the edges acting as the active sites [59]. The nitrogen molecules are shown to preferably adsorb on the edges rather than the basal planes and thus the N_2 fixation can be enhanced by engineering their edges. Reports made by Sun et. al. and others have theoretically and experimentally demonstrated that the defects and Mo edges of the 2D MoS_2 nanostructure play an important role in N_2 adsorption, polarization, and activation [60,61].

In 2017, Sun and coworkers carried out the first experimental confirmation of photocatalytic N_2 fixation to ammonia on MoS_2 [30]. They developed ultrathin MoS_2 nanosheets with a thickness of about 3.5 nm and a high ammonia production rate of 325 μmol $g^{-1}h^{-1}$ was obtained under visible light without the use of scavengers. The photocatalytic activity was shown to be induced by charged excitons formed on the ultrathin MoS_2 nanosheets acting as electron rich species (Fig. 7). Due to the strong quantum confinement in ultrathin transition metal dichalcogenides (TMDs), the strong coulomb interactions cause the formation of tightly bound excitons from photoexcited electron-hole pairs [62,63]. This leads to formation of charged excitons (such as trions) by capturing of additional electrons by tightly bound excitons and can act as electron-rich species to facilitate multielectron N_2 reduction process [62]. A large amount of sulfur vacancies also exists on the surface of the ultrathin MoS_2 nanosheets and is believed to capture the N_2 molecules facilitating its activation. This study has an implication of an exceptional advantage of electron rich systems having high concentration of localized electrons in N_2 activation and reduction.

Strategies involving the regulation of edges for better exposure of active sites as well as the modulation of interaction between Mo and NH_x species is crucial in developing efficient MoS_2 photocatalysts. Recently, Hu et al. theoretically proposed rational design of active sites of MoS_2 by regulating the edge sites using Mn as a dopant [64]. The Mn doping was shown to change inert S edge sites to active sites by forming S vacancies and thus resulting in higher exposure of Mo edge sites. The fabricated Mn-doped MoS_{2-x} nanoflowers with optimal Mn content displayed excellent photocatalytic performance, achieving an ammonia yield of 213.2 μmol $g^{-1}h^{-1}$ in pure water without the use of sacrificial agent under full light irradiation. This activity is 5.3 times higher than that of the pristine MoS_2 (40.2 μmol $g^{-1}h^{-1}$) and is supe-

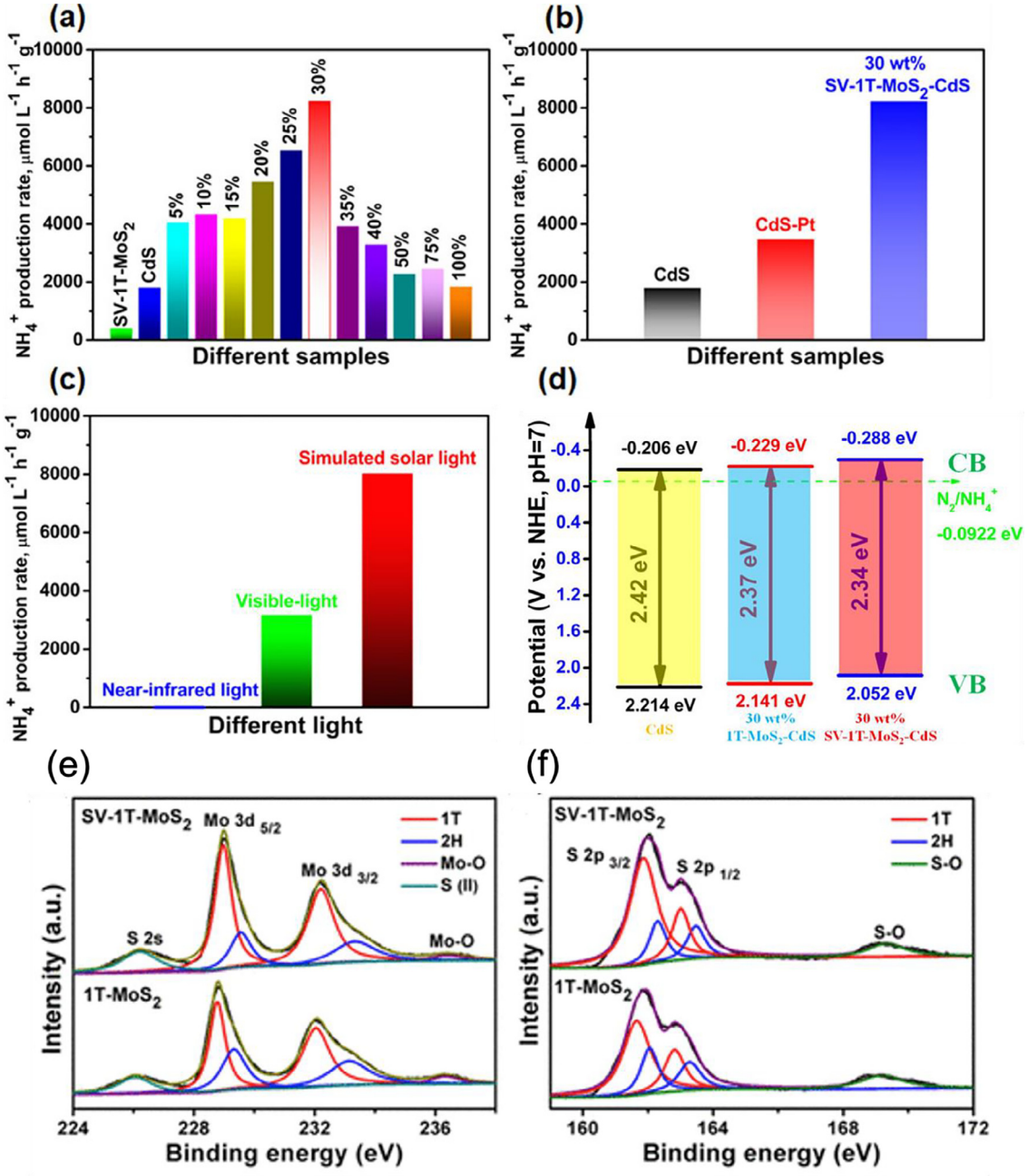

Fig. 5. Photocatalytic NH_4^+ production rates of (a) SV-1T-MoS_2, CdS nanorods, and SV-1T-MoS_2/CdS composites containing different amounts of SV-1T-MoS_2, (b) CdS nanorods, CdS-Pt (0.1 wt%), and 30 wt% SV-1T-MoS_2/CdS composites under simulated solar light irradiation, (c) 30 wt% SV-1T-MoS_2/CdS composites under different light irradiation, (d) Band structure of CdS, 30 wt% 1T-MoS_2/CdS, and 30 wt% SV-1T-MoS_2/CdS composites, and high-resolution XPS spectra of (e) Mo 3d, and (f) S 2p. Reproduced with permission from Ref. [52]. Copyright 2020, American Chemical Society.

rior to most of the reported MoS_2-based photocatalysts. The Mn doping creates rich planar defects on MoS_2 and lowers the energy barriers thus facilitating N_2 adsorption and activation by elongating the N≡N bond.

Crystal phase engineering in transition-metal dichalcogenides is a powerful strategy to develop efficient photocatalysts and tuning their catalytic activities [103–106]. MoS_2 generally exists in two phases, stable hexagonal (2H) semiconducting phase and metastable trigonal (1T) metallic phase. The 1T-MoS_2 is highly conductive and has more active sites, facilitating fast electron/charge transfer, which leads to much higher catalytic activity than the 2H-MoS_2.Thus, to make use of both stability and higher activity, it is imperative to design a multiphasic catalyst (1T/2H MoS_2) by controlling the concentration of the phases [65,66]. Xu and coworkers proposed ultrathin alloyed mixed-phase $Mo_{1-x}W_xS_2$ nanosheets synthesized by a one-step hydrothermal method with controlled 2H/1T phase ratios [67]. The $Mo_{1-x}W_xS_2$ with 33.6 % of 1T phase concentration and Mo/W = 0.68:0.32 (MWS-2) displays an optimum photocatalytic performance with an NH_3 production rate of about 111 μmol $g_{cat}^{-1}h^{-1}$ under visible light irradiation and using Na_2SO_3 as a scavenger (Fig. 8(a) & (b)). This N_2 fixation rate is 3.7 (or 3) times more than that of the pristine MoS_2 (or WS_2) nanosheets. The DFT calculations and in situ N_2 absorption XANES together with the N_2-TPD (Fig. 7(c)) show that the W doping promote the N_2 adsorption process and induces the change of interfacial electric density. The synergistic effect of the optimum ratio of the mixed-phase 2H/1T structure and W doping accounts for the high photocatalytic activity of the $Mo_{1-x}W_xS_2$ nanosheets (Table 2. Table 3.

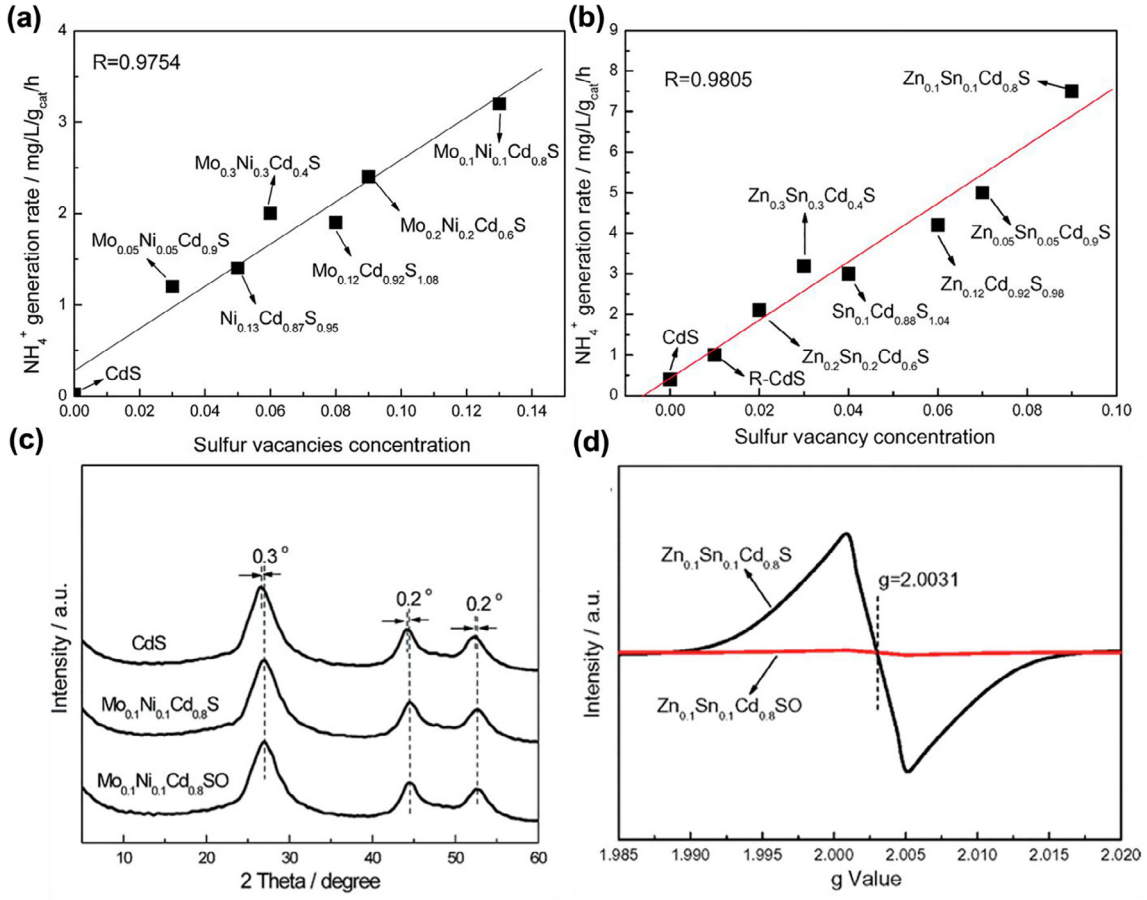

Fig. 6. Dependence of photocatalytic N_2 fixation performance on the concentration of sulfur vacancies in CdS-based materials doped with (a) Zn and Sn or (b) Mo and Ni. For (a), reproduced with permission from ref. [56]. Copyright 2016, Royal Society of Chemistry. For (b), reproduced with permission from ref. [55]. Copyright 2016, Royal Society of Chemistry. (c) The XRD patterns of $Mo_{0.1}Ni_{0.1}Cd_{0.8}S$ and $Mo_{0.1}Ni_{0.1}Cd_{0.8}SO$ (d) EPR spectra of $Zn_{0.1}Sn_{0.1}Cd_{0.8}S$ and $Zn_{0.1}Sn_{0.1}Cd_{0.8}SO$.

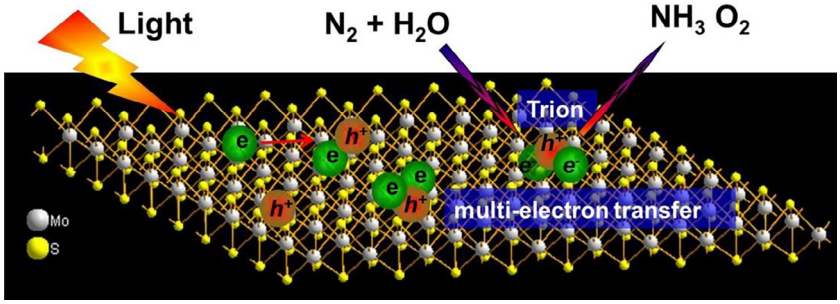

Fig. 7. Schematic of the trion-induced multi-electron N_2 reduction process. Reproduced with permission [30]. Copyright 2017, Elsevier.

Another effort was recently made to use MoS_2 as an effective photocatalyst for nitrogen fixation enhanced by non-metal doping and use of a noble metal Pt co-catalyst [68]. The flower like *N*-doped MoS_2 microspheres were made by self-assembly of nanosheets, which is advantageous providing more active sites and ultimately improving the N_2 fixation. The Pt/N-MoS_2 displayed improved N_2 photofixation compared to the pure MoS_2 owing to the band gap narrowing by *N*-doping and accelerated charge transfer and carrier separation by the Pt co-catalysts. Moreover, the authors suggested the promise of using ultrasonic method to facilitate N_2 fixation and that the synergistic effect of sonocatalysis and photocatalysis further improves the activity.

Shi et al. [69] recently reported WS_2@TiO_2 nanoporous films (NFs) prepared by using a facile method. Here, the WS_2 nanoflakes are used as attractive cocatalysts for the first time to promote photocatalytic fixation of N_2. They were deposited inside the nanopores of the oxygen vacancy TiO_2 film. The WS_2@TiO_2 NFs with a 20 % WS_2 loading display highly outstanding performance with an outstanding NH_3 yield rate of 1.39 mmol $g^{-1}h^{-1}$ under simulated sunlight irradiation. The WS_2@TiO_2 NFs heterojunctions formed enhance charge separation efficiency and prolong the lifetime of charge carriers. The oxygen vacancy on the surface of TiO_2 plays a big role by providing binding site for N_2 adsorption.

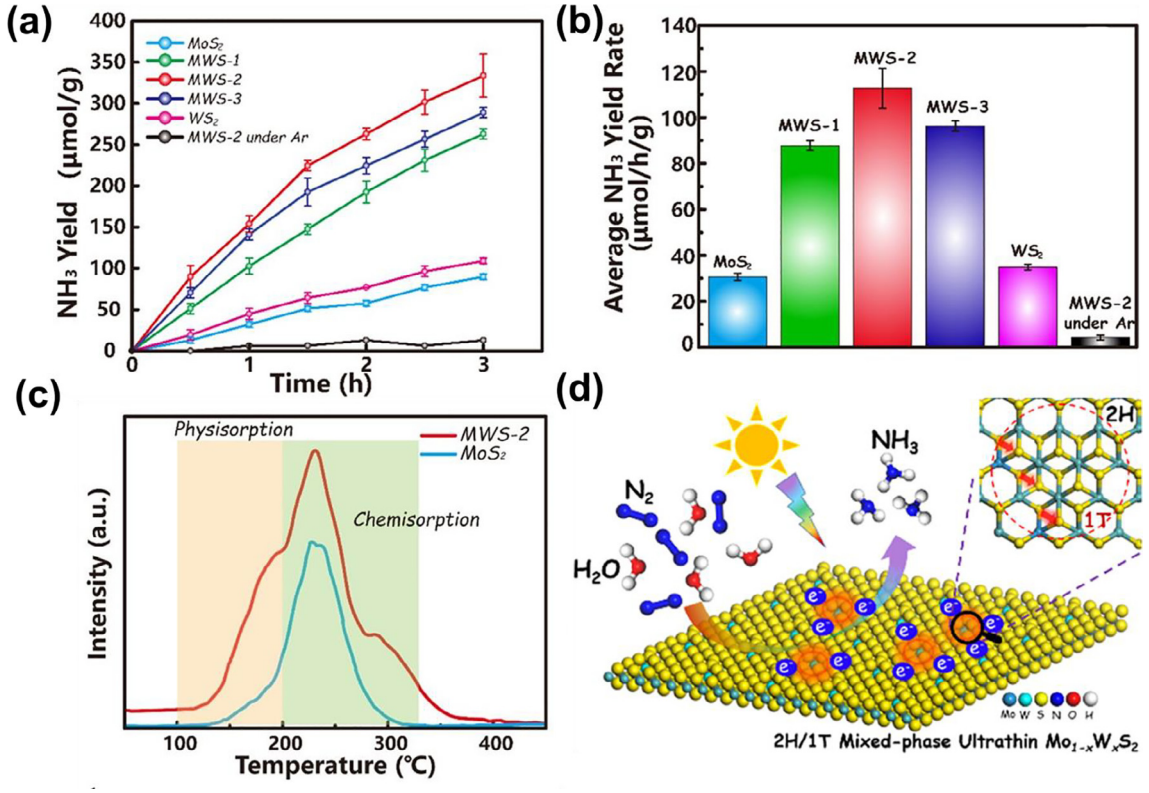

Fig. 8. (a) Corresponding time course of the NH_3 yield rate over different catalysts under the visible-light irradiation; (b) comparison of the NH_3 yield rate; (c) N_2-TPD profiles of MoS_2 and MWS-2; (d) scheme for photocatalytic N_2 reduction over 2H/1T $Mo_{1-x}W_xS_2$ nanosheets. Reproduced with permission from [67]. Copyright 2021, American Chemical Society.

3.3. Indium-based sulfides

Indium based sulphides are well known visible-light-responsive semiconductors with exceptional absorption coefficient, excellent carrier mobility, reasonable band gap, chemical stability and low toxicity [70–73]. Different approaches were devised to improve its photocatalytic property such as introducing surface defects and forming heterojunctions [73–76].

He and coworkers designed In_2S_3 nanotubes containing sulfur vacancies formed by thermal treatment under nitrogen atmosphere [33]. The constructed sulfur vacancies in In_2S_3 resulted in enhanced photocatalytic performance with NH_3 yield rate of 52.49 μmol $g^{-1}h^{-1}$. This enhancement is due to an accelerated photogenerated charge separation efficiency. In another study, these same group of researchers reported In_2O_3/In_2S_3 microsphere heterostructures prepared by a simple two-step hydrothermal process [76]. Flakes of In_2S_3 were formed in situ and assembled on the In_2O_3 microsphere host. The photocatalytic N_2 fixation activity of In_2O_3/In_2S_3 heterostructure was significantly improved and achieved fixation rate of 40.04 μmol $g^{-1}h^{-1}$ under UV–vis light irradiation. This activity is higher than that of the pure In_2O_3 and In_2S_3, respectively (Fig. 9(a)). The enhanced photocatalytic nitrogen fixation is ascribed to the construction of heterostructures with strong interfacial contact, which increases the oxygen vacancies as shown in the ESR spectra (Fig. 9(b)) and extends the light absorption range. The oxygen vacancies act as trap states accepting photon-generated electrons and thus promote charge transfer and separation efficiency (Fig. 9(c)).

Ternary indium sulfides are another class of indium-based sulfides that are of current interest [77]. As the ternary indium sulfides have outstanding electronic and optical properties and chemical stability, they have potential applications in various photocatalytic fields such as H_2 evolution [78], CO_2 reduction [79], and C—C coupling [80,81]. Among them, the zinc indium sulfides (Zn-In-S) are the most important visible-light-responsive photocatalysts in this family [82,83]. Han *et. al.* synthesized 3D nanosheet-assembled $Zn_3In_2S_6$ spheres with rich zinc vacancies (V_{Zn}) as a highly active photocatalyst for nitrogen fixation [84]. The zinc defect V_{Zn}-$Zn_3In_2S_6$ achieved NH_4^+ production of 355.2 mg L^{-1} g_{cat}^{-1} after 4 h reaction under visible light irradiation, a much higher activity than the bulk $Zn_3In_2S_6$ with poor V_{Zn}. The greatly enhanced photocatalytic activity is mainly due to the V_{Zn} and the unique 3D multi-staged nanosheet structure, which accelerate charge carrier separation and transport and generate more surface-active sites enhancing photocatalytic efficiency. In another study, Swain et al. [85] developed 2D-2D type p-MoS_2/n-$MgIn_2S_4$ heterojunction with a flower-like morphology by a two-step hydrothermal method. The heterojunction displayed an enhanced photocatalytic NH_3 production by controlling the loading of MoS_2. A photocatalytic NH_3 yield of 0.81 mg/L was achieved for 5 % MoS_2/MIS in pure water, which is 4.05 and 6.75 times more than that of bare MoS_2 and MIS, respectively. The NH_4^+ generation is observed to be more efficient in 10 vol% methanol–water solution serving as a sacrificial agent and achieved a NH_4^+ yield of about 1.54 mg/L. The p-n heterojunction provides large reactive sites for the photocatalytic N_2 activation and provides a suitable pathway for the efficient reduction of nitrogen.

3.4. Metal sulfide/carbon heterostructures

Heterostructure photocatalysts contain interfaces that helps in employing the distinctive properties of the components and synergistic effects between them [86,87]. The heterojunction constructed helps in fast charge transfer and separation and enhances light absorption. Owing to their enhanced electronic conductivity, high surface area and chemical stability, carbon-based heterojunction photocatalysts are attractive materials for nitrogen photofixation.

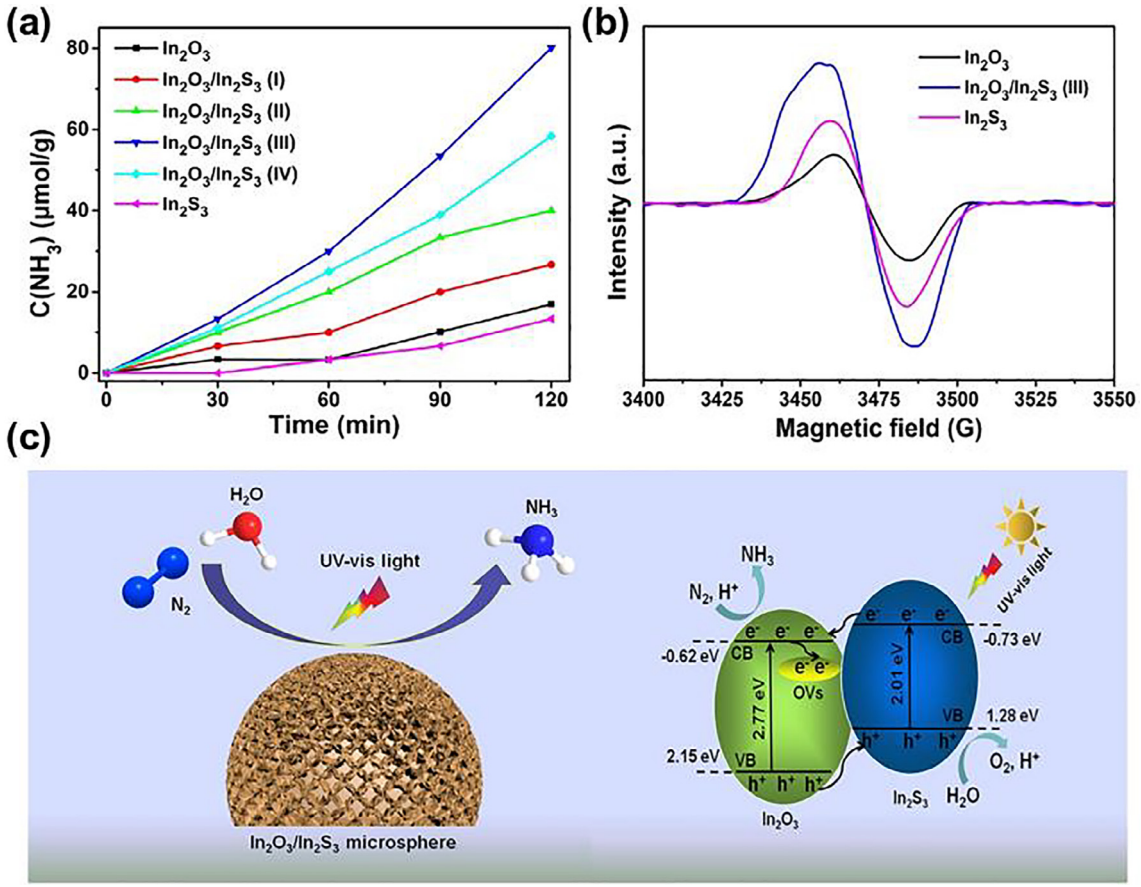

Fig. 9. Determination of the generated NH_3 under UV–vis light (b) ESR spectra of pure In_2O_3, In_2O_3/In_2S_3 (III) heterostructure and In_2S_3 (c) Schematic diagram showing the mechanism for photocatalytic nitrogen fixation. Adapted with permission from [76]. Copyright 2019, Elsevier.

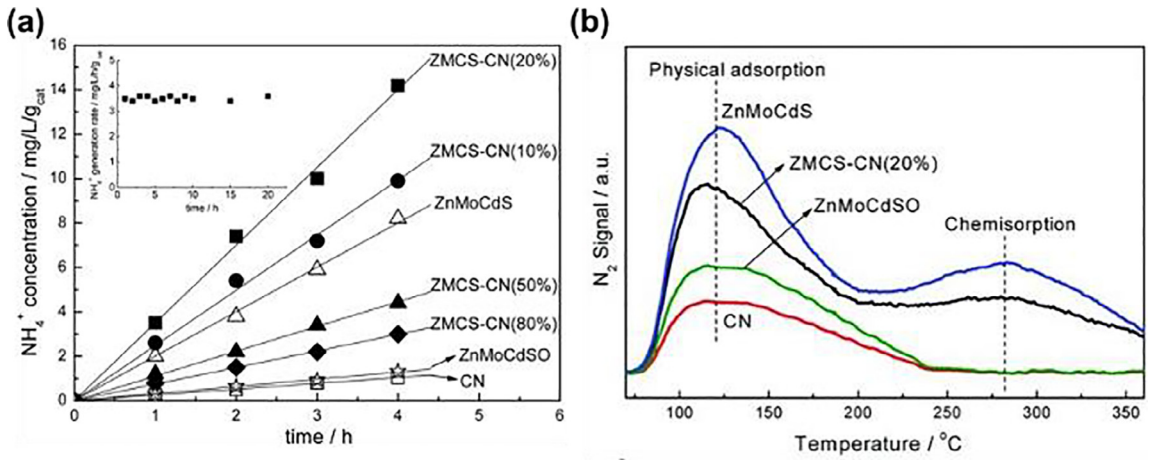

Fig. 10. (a) Nitrogen photofixation performance over the as prepared catalysts under visible light, (b) The N_2-TPD of CN, ZnMoCdS, ZnMoCdSO and ZMCS-CN (20 %), and (c) The schematic illustration of electron-hole separation and transport at the g-C_3N_4/ZnMoCdS heterojunction interface. Reproduced with permission from [88]. Copyright 2016, Royal Society of Chemistry.

Zhang et al. prepared a heterojunction g-C_3N_4/ZnMoCdS by post-treatment of g-C_3N_4 hydrothermally with the metal precursors and sulfur source [88]. The heterojunction with an optimum 80 % by weight of ZnMoCdS displays the maximum NH_4^+ production rate under visible light (Fig. 10(a)). The prepared ZnMoCdS ternary metal sulfide has a composition of $Zn_{0.12}Mo_{0.12}Cd_{0.9}S_{1.14}$ and possesses many sulfur defects, which function as active sites to adsorb and reduce N_2 molecules. N_2 is strongly adsorbed on ZnMoCdS and ZMCS-CN (20 %) suggesting that the nitrogen photofixation occurs on the ZnMoCdS (Fig. 10(b)). Therefore, the superior nitrogen photofixation ability of the composite is ascribed to the heterojunction formation and sulfur vacancies. In a similar study, these researchers reported another ternary metal sulfide ZnSnCdS coupled to g-C_3N_4 forming a heterojunction [89]. The ternary metal sulfide with defects of sulfur vacancies and composition $Zn_{0.11}Sn_{0.12}Cd_{0.88}S_{1.12}$ plays the main role in the enhancement of the photocatalytic activity of the heterojunction. The hetero-

Table 2
Recent advances in transition metal sulfide-based photocatalysts for nitrogen fixation.

Photocatalyst	Light source	Sacrificial agent	Ammonia production rate (μmol $g^{-1}h^{-1}$)	Quantum efficiency	Ref.
Ultrathin MoS_2 nanosheets	500 W Xe lamp, >420 nm	None	325		[30]
Pt/N-MoS_2	300 W Xe lamp, >420 nm	Methanol	121.2		[68]
Mn-MoS_{2-x}	300 W Xe lamp	None	213.2	0.26 % @ 350 nm	[64]
MoS_2/n-$MgIn_2S_4$	250 W Hg lamp	Methanol	142.6		[85]
$Mo_{1-x}W_xS_2$ nanosheets	300 W Xe lamp, > 400 nm	Na_2SO_3	111	0.09 % @ 420 nm	[67]
WS_2@TiO_2 film	AM 1.5G	Na_2SO_3	1390		[69]
$Zn_{0.8}Cd_{0.2}S$	300 W Xe lamp	Na_2SO_3	66.91	3.77 % @ 420 nm	[49]
SV-1T-MoS_2-/CdS	AM 1.5G	Methanol	822.08	4.42 %	[52]
NiS/CdS	300 W Xe lamp	None	94.4	0.76 % @ 420 nm	[51]
BPNS/CdS	300 W Xe lamp, >420 nm	Methanol	240.17		[32]
$Ni_2P/Cd_{0.5}Zn_{0.5}S$	300 W Xe lamp, >420 nm	None	254	4.32 % @ 420 nm	[50]
$Mo_{0.1}Ni_{0.1}Cd_{0.8}S$	250 W Na lamp	Ethanol	88.89		[55]
$Zn_{0.11}Sn_{0.12}Cd_{0.88}S_{1.12}$/g-$C_3N_4$	250 W Na lamp, >420 nm	Ethanol	209.5		[89]
g-C_3N_4/ZnMoCdS	250 W Na lamp, >420 nm	Ethanol	97.2		[88]
In_2O_3/In_2S_3 microsphere	300 W Xe lamp	None	40.04		[76]
In_2S_3 nanotubes	300 W Xe lamp	None	52.49		[33]
$Zn_3In_2S_6$ nanosheets	300 W Xe lamp, >420 nm	Methanol	246.67		[84]
FeS_2/CNT	Xe lamp	None	67.35	0.41 % @ 367 nm	[93]

Table 3
Recent advances in transition metal sulfide-based electrocatalysts for nitrogen fixation.

Catalyst	Electrolyte	Potential (V vs RHE)	NH_3 yield	FE (%)	Ref.
MoS_2	0.1 M Na_2SO_4	−0.5	8.08×10^{-11} mol s^{-1} cm^{-2}	1.17	[61]
Defect rich MoS_2 nanoflowers	0.1 M Na_2SO_4	−0.4	29.28 μg h^{-1} $mg_{cat.}^{-1}$	8.34	[60]
V_S-MoS_2	0.1 M Na_2SO_4	−0.5	46.1×10^{-11} mol s^{-1} cm^{-2}	4.58	[104]
WS_{2-x} nanosheets	0.1 M Na_2SO_4	−0.6	16.38 μg h^{-1} mg_{cat}^{-1}	12.1	[105]
CoS_{1-x}	0.05 M H_2SO_4	−0.15	12.1 μg h^{-1} mg_{cat}^{-1}	16.5	[106]
VS_2-350	0.1 M HCl	−0.6	20.29 μg h^{-1} mg_{cat}^{-1}	3.86	[107]
MoS_2-V	0.1 M Na_2SO_4	−0.35	20.11 μg h^{-1} mg_{cat}^{-1}	15.72	[109]
FeS_2-Mo	0.1 M KOH	−0.2	26.15 μg h^{-1} mg_{cat}^{-1}	14.41	[110]
Co-doped MoS_{2-x}	0.01 M H_2SO_4	0.3	0.63 mmol $h^{-1}g^{-1}$	10	[111]
Mo-SnS_2-Vs	0.5 M $LiClO_4$	0.5	41.3 μg h^{-1} mg_{cat}^{-1}	20.8	[112]
Fe-ReS_2@*N*-CNF	0.1 M Na_2SO_4	−0.2	80.4 μg h^{-1} mg_{cat}^{-1}	12.3	[115]
N-doped MoS_2	0.1 M Na_2SO_4	−0.3	69.82 μg h^{-1} mg_{cat}^{-1}	9.14	[119]
P-doped MoS_2	0.1 M Na_2SO_4	−0.6	60.27 μg h^{-1} mg_{cat}^{-1}	12.22	[120]
B-VS_2	0.5 M $LiClO_4$	−0.4	55.7 μg h^{-1} mg_{cat}^{-1}	16.4	[121]
F-MoS_2	0.05 M H_2SO_4	−0.2	35.7 μg h^{-1} mg_{cat}^{-1}	20.6	[122]
FeS@MoS_2	0.1 M Na_2SO_4	−0.5	8.45 μg h^{-1} cm^{-2}	2.96	[124]
FeS_2-MoS_2@IF_{200}	0.1 M KOH	−0.5	7.1×10^{-10} mol s^{-1} cm^{-2}	4.6	[125]
CoS_2/MoS_2	0.1 M Li_2SO_4	−0.6	54.7 μg h^{-1} mg_{cat}^{-1}	20.8	[126]
$FeNi_2S_4$/NiS	0.1 M KOH	−0.3	128.4 μg h^{-1} cm^{-2}	28.64	[127]
$Fe_{3\%}$-$Cu_{2-x}S$ QDs	0.1 M Na_2SO_4	−0.7	26.4 μg h^{-1} mg_{cat}^{-1}	3.1	[128]
NPG@SnS_2	0.1 M Na_2SO_4	−0.6	20.72 μg h^{-1} cm^{-2}	49.3	[131]
AuNPs@MoS_2	0.1 M KOH	−0.3	25 mg h^{-1} mg_{cat}^{-1}	9.7	[132]
Ru/2H-MoS_2	0.01 M HCl	−0.2	6.7×10^{-11} mol cm^{-2} s^{-1}	17.6	[133]
SACs-MoS_2-Fe	0.1 M KCl	−0.2	97.5 mg h^{-1} cm^{-2}	31.6	[136]
MoS_2/g-C_3N_4	0.1 M $LiClO_4$	−0.3	18.5 μg h^{-1} mg^{-1}	17.8	[137]
CoS_x/NS-G	0.05 M H_2SO_4	−0.2	25.0 μg h^{-1} mg_{cat}^{-1}	25.9	[138]
NiCoS/C	0.1 M Li_2SO_4	0	26.0 μg h^{-1} mg^{-1}	12.9	[143]
$Fe_2Mo_6S_8$	0.5 M Na_2SO_4	−0.2	70 μg h^{-1} mg_{cat}^{-1}	12.5	[141]
Re_2MnS_6	0.1 M Na_2SO_4	−0.3	3.78 μg h^{-1} mg_{cat}^{-1}	17.42	[142]

junction with 80 % by weight of ZnSnCdS displays the highest NH_4^+ production rate.

The nitrogenase in nature has essentially iron-sulfur nanoclusters as active sites for nitrogen fixation [90]. As a bio-inspired material, Iron pyrite (FeS_2), has been proven to have nitrogen fixing ability owing to the similar ligand field structure of its iron atom to natural nitrogenase [91,92]. Lashgaria et al. synthesized FeS_2 through a solvothermal route in the presence of carbon nanotube (CNT) as an effective and narrow-bandgap photocatalyst for N_2-photofixation under ambient conditions [93]. The composite FeS_2/CNT is shown to be an effective photocatalyst by displaying an ammonia production rate of around 750 μmol/L $g^{-1}h^{-1}$, twice as the bare FeS_2 without any scavenger. The presence of CNT in the composite adjusts the energy band positions and boosts the absorption of photons, increases the surface area, and thus improves the charge separation. This study suggests the importance of carbon support materials in improving and stabilizing the photocatalytic activity of solar-energy materials.

Other heterostructures and heterojunctions of metal sulfides with other materials are also reported, which offer enhanced photocatalytic performance. For example, Chen and colleagues investigated heterojunction composites of Bi_2S_3, CuS, Ag_2S, and NiS with perovskite-structured $KNbO_3$ and $KTa_xNb_{1-x}O_3$ oxides prepared by optimizing the metal sulfide loadings [94–98]. These composite heterostructures demonstrated high efficiency in the photocatalytic reduction of N_2 to NH_3. The metal sulfides displayed an obvious promotion effect on $KNbO_3$ under light irradiation because the heterojunction formed at

the contact interface of metal sulfides and $KNbO_3$ greatly improved the separation efficiency of electron-hole pairs. In addition to the high photocatalytic performance, these materials have a remarkable piezocatalytic activity suggesting the synergistic effect of the two processes in enhancing the overall catalytic N_2 fixation [98]. In another study Xing et al. [99] reported a ternary MoS_2/C-ZnO composite prepared by a combination of hydrothermal synthesis of C-ZnO and photodeposition of MoS_2 nanoparticles on the C-ZnO. The carbon layer formed on the surface of ZnO acts as a photosensitizer to transfer electrons to ZnO or MoS_2 and the MoS_2 is shown to further enhance the separation of electron-hole pairs by trapping electrons. Table 2 summarizes the recently reported metal sulfide-based photocatalysts for nitrogen fixation comparing the their performance.

4. Recent advances in metal sulfide-based electrocatalysts

Metal sulfide-based materials are widely employed as effective electrocatalysts for the nitrogen fixation under ambient conditions owing to their resemblance to the nitrogenase. Recently, various transition metal sulfide electrocatalysts have been developed with promising NRR activity (Table 3). However, the NH_3 production and faradaic efficiency (FE) is still low due to sluggish reaction kinetics, the inertness of N_2 molecules, and the competing hydrogen evolution reaction (HER). Thus, it is imperative to design strategies to boost the intrinsic NRR activity and enhance efficiency of these electrocatalysts. Various strategies have been employed including defect engineering [100], heteroatom doping [101], interfacial engineering, and construction of metal sulfides with multi active sites.

4.1. Defect engineering

Defect engineering is important in tuning the electronic structure of electrocatalysts in order to provide ample active sites and improve the intrinsic activity. This is essential to realize excellent NRR activity and boost the faradaic efficiency [100,102]. Sulfur vacancies defects are the most investigated defect types for metal sulfides and have been demonstrated to efficiently adsorb N_2. The primary role of the sulfur vacancies is to regulate the electronic structure of the catalyst and boost donation of electrons from the metal back to the N_2 antibonding orbitals so as to activate the N≡N triple bond effectively [103].

MoS_2, as the most important class of 2D chalcogenide material, has been widely investigated for its NRR activity and the role of sulfur defects on its activity by engineering the edges [59]. Sun et al. [61] first proved theoretically and experimentally MoS_2 as an active electrocatalyst for nitrogen fixation. A NH_3 yield rate of 8.08×10^{-11} mol s^{-1} cm^{-2} and FE of 1.17 %, is achieved at −0.5 V in 0.1 M Na_2SO_4. The theoretical studies demonstrated that the MoS_2 edges appears to be the active site for the NRR. Nevertheless, the FE is very low due to the competing HER and thus engineering the edge sites by creating defects is considered as an effective strategy to improve the activity. Li et al. prepared defect rich MoS_2 nanoflowers and it achieved FE of 8.34 % and NH_3 yield of 29.28 μg h^{-1} $mg_{cat.}^{-1}$ at −0.40 V in 0.1 M Na_2SO_4 [60]. The activity is higher than the counterpart without defects (13.41 μg h^{-1} $mg_{cat.}^{-1}$ and 2.18 %). The defect introduced to MoS_2 nanoflowers is shown to provide lower energy barrier than the defect free MoS_2. Recently, Ma and coworkers synthesized sulfur-vacancies defected MoS_2 (V_S-MoS_2) with excessive Mo atoms displaying a great potential for NRR [104]. The V_S-MoS_2 attained NH_3 production rate of 46.1×10^{-11} mol s^{-1} cm^{-2} at −0.5 V and FE of 4.58 % at −0.4 V suggesting that the Mo exposed due to sulfur vacancy defects enhances the NRR activity.

WS_2 nanosheets like MoS_2 can be modified by defects to expose more metal sites to boost its NRR activity. Ma et al. prepared WS_{2-x} nanosheets with rich sulfur defects by calcining oxygen vacancy WO_3 in the presence of sulfur and boron under vacuum [105]. The WS_{2-x} displayed NH_3 production rate of 16.38 μg h^{-1} $mg_{cat.}^{-1}$ and high FE of 12.1 % at −0.6 V in 0.1 M Na_2SO_4 solution. The WS_{2-x} nanosheets were observed to achieve high durability and structural stability after catalytic reaction.

Cobalt sulfide is another potential transition metal sulfide electrocatalyst, which can be used as a suitable catalyst for NRR by constructing sulfur vacancies owing to the existence of Co^{2+}/Co^{3+} redox pairs. Li et al. designed CoS nanoflowers with abundant sulfur vacancies (CoS_{1-x}) by Ar-plasma treatment of the as prepared CoS [106]. An enhanced NRR activity with FE of 16.5 ± 1.5 % and NH_3 yield rate of 12.1 ± 1.4 μg h^{-1} mg_{cat}^{-1} is obtained in 0.05 M H_2SO_4. The sulfur vacancies in CoS_{1-x} boost the NRR activity by effectively suppressing HER and the exposed Co selectively adsorbs N_2 molecules.

Most of the research works on transition metal sulfide based NRR electrocatalysts give stronger emphasis to elucidating the metal atoms as active sites. But, the role of S sites has not been given enough attention, and the strategy of modifying S sites is rarely investigated. Recently, Zhao et al. designed VS_2 by removing S edges by a thermal treatment at 350 °C and keeping the structure of VS_2 edges intact [107]. The as-prepared VS_2-350 electrocatalyst demonstrates NH_3 production rate of 20.29 μg h^{-1} mg_{cat}^{-1} at −0.6 V in 0.1 M HCl, better than the untreated VS_2. The promising NRR activity of VS_2-350 is ascribed to the more exposed V atoms and suppressed HER caused by removing S edges.

4.2. Heteroatom doping

4.2.1. Metal doping

Heteroatom doping can also be used in the optimizing the electronic structure of electrocatalytic materials and tuning the adsorption of N_2 molecules [108]. Niu et al. studied the role of Fe and V dopants on MoS_2 prepared by in situ doping to understand the relationship between nitrogen adsorption, nitrogen activation and ammonia desorption in the NRR process [109]. It is shown that the V-doped MoS_2 (MoS_2-V) displays better nitrogen adsorption and activation, while Fe-doped MoS_2 (MoS_2-Fe) attains higher ammonia production rate of 20.11 μg h^{-1} mg_{cat}^{-1} at −0.35 V (Fig. 11). Thus, the Fe-doped MoS_2 exhibited a better balance in terms of N_2 adsorption and activation and NH_3 desorption. This indicates the need for the optimal balance between the three key steps of NRR to achieve the best performance. In another study, Wang and.

coworkers designed a biomimetic electrocatalyst by doping Mo(IV) on FeS_2 (FeS_2-Mo) [110]. The Mo doped FeS_2 exhibits FE of 14.41 % at −0.2 V and a NH_3 yield rate of 26.15 μg h^{-1} mg_{cat}^{-1} higher than the undoped FeS_2. Thus, the Mo^{4+} dopant acts as an active site and boosts the N_2 adsorption and its subsequent activation.

A strategy combining heteroatom doping and vacancy engineering is employed to bring synergistic effect of creating more active sites and tuning the electronic properties of catalysts. Zhang et al. demonstrated that sulfur vacancy (Vs) MoS_{2-x} nanosheets tailored by Co doping present excellent NRR activity [111]. The Co-doped MoS_{2-x} attained an ammonia yield rate of 0.63 mmol $h^{-1}g^{-1}$ and a FE of over 10 % at an overpotential of 0.3 V. The outstanding activity of Co-doped MoS_{2-x} is due to the combined effect of metal doping and vs which facilitates N_2 adsorption and efficient N_2 activation. Chu et al. used this strategy to prepare Mo-doped SnS_2 (Mo-SnS_2-Vs), which caused the generation of sulfur vacancy defects (Vs) [112]. The Mo-doped SnS_2 nanosheets displayed high NH_3 yield of 41.3 μg h^{-1} mg_{cat}^{-1} at 0.5 V and a FE of 20.8 % at 0.4 V in 0.5 M $LiClO_4$. The DFT studies have revealed that the Mo-SnS_2-vs shows unique NRR mechanism proceeding through an enzymatic pathway and enhanced activity due to the formation of Mo–Sn–Sn trimer active sites.

Rhenium disulfide (ReS_2), as a 2D transition metal dichalcogenide has recently attracted research interest as highly efficient electrocatalyst due the weak interactions between the layers [113,114]. Lai et al. proposed doping transition metals (Fe, Co, Ni, Cu, Zn) with low

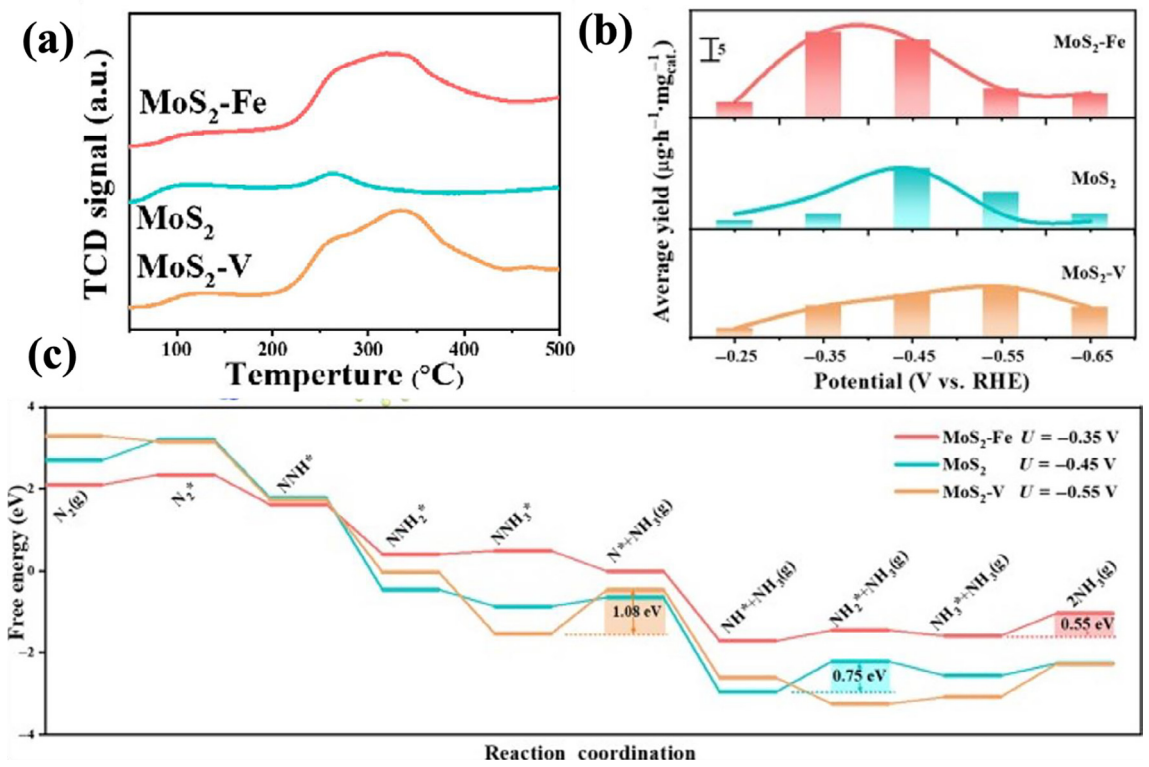

Fig. 11. (a) N_2 TPD profiles of MoS_2-Fe, MoS_2, and MoS_2-V. (b) Average NH_3 yields of MoS_2-Fe, MoS_2, and MoS_2-V at different potentials. (c) Free-energy profiles of the NRR of MoS2-Fe (red line), MoS_2 (blue line) and MoS_2-V (orange line) at −0.35, −0.45, and −0.55 V, respectively. Reproduced with permission from [109]. Copyright 2021, Springer Nature. (For interpretation of the references to colour in this figure legend, the reader is referred to the web version of this article.)

valency in to ReS_2 to tune its energy levels, which creates enhanced charge density around the dopants [115]. It is demonstrated that Fe-doped ReS_2 nanosheets exhibits excellent NRR activity with eightfold more ammonia production of 80.4 μg h^{-1} mg_{cat}^{-1} (FE = 12.3 %) than the pristine ReS_2 at −0.2 V in 0.1 M Na_2SO_4. The boosted NRR activity can be ascribed to the introduction of dopants in to the ReS_2 structure forming an active site for adsorption and optimal activation of N_2.

4.2.1.1. Non-metal doping. Similar to metal doping, non-metal doping have also been widely used to modify electrocatalysts to bring about charge redistribution on the surface to adjust the NRR activity [116–119].

Zeng and colleagues developed *N*-doped MoS_2 nanoflowers having rich sulfur vacancies for efficient NRR [119]. The *N*-doped MoS_2 nanoflowers offered an outstanding NH_3 yield of 69.82 μg h^{-1} mg_{cat}^{-1} and a high FE of 9.14 % at −0.3 V in 0.1 M Na_2SO_4 solution. The excellent performance of the *N*-doped MoS_2 is due to the sulfur vacancies created and formation of Mo-N active sites upon N doping and thus facilitating electron transfer and enhancing N_2 activation. Recently, Fei et al. constructed P-doped MoS_2 with rich sulfur vacancy by a simple hydrothermal method [120]. The optimized P-doped MoS_2 catalyst attained an NH_3 production rate of 60.27 μg h^{-1} mg_{cat}^{-1} and a large FE of 12.22 % at −0.6 V in 0.1 M Na_2SO_4 (Fig. 12). The P doping created.

rich vs in MoS_2 and regulated the defect level as it is evident from the N_2 TPD and (Fig. 12(a)) and increased the electrochemical active surface area (ECSA), as well (Fig. 12(d)). Thus, the doping is shown to enhance the N_2 adsorption and activation significantly. In a similar trend, Li and coworkers simultaneously constructed S-vacancies (Vs) and introduced B-dopants into VS_2 to activate its basal planes [121]. The B-doped VS_2 nanoflower achieved an NH_3 production rate of 55.7 μg h^{-1} mg_{cat}^{-1} at −0.4 V and an FE of 16.4 % at −0.2 V making it one of the best V-based electrocatalysts reported. The researchers demonstrated that the S-vacancies (Vs) and B-dopants work synergistically by creating unique B-adjacent-unsaturated-V active sites to successfully enhance the nitrogen reduction and inhibit the competitive HER (Fig. 13.. Fig. 14).

Another approach used to introduce defects is by strain engineering, which is meant to alter the interlayer spacing of crystal structures, thus enhancing the activity and efficiency of the catalysts. Liang et al. developed strain induced defect MoS_2 by introducing F^- into the interlayer of MoS_2 [122]. The F-MoS_2 shows superior NRR activity with NH_3 production rate of 35.7 μg h^{-1} mg_{cat}^{-1} and a high FE of 20.6 % at −0.2 V. The high NRR activity is due to the reduction of HER and formation of more active sites upon F doping.

4.3. Interfacial engineering

Interface engineering is an important strategy that helps to modulate the electrocatalytic activity of catalysts. Interfaces allow accelerated charge transfer and adjusted free energies of intermediates due to the strong interfacial interactions of components [123]. Owing to the poor electronic transfer and agglomerations of transition metal-based catalysts, which reduces the active sites, the NRR activity of single component electrocatalysts is generally unsatisfactory.

4.3.1. Metal sulfide/metal sulfide interface

Constructing metal sulfide/metal sulfide heterojunctions is an effective strategy to create interfaces in metal sulfide based electrocatalysts. Guo et al. prepared FeS@MoS_2 hybrid catalyst via a one-step hydrothermal method with FeS nanoparticles homogeneously distributed on the MoS_2 nanosheets [124]. Due to the synergy between the Fe and Mo active sites and conductive CFC support, the FeS@MoS_2/CFC with an optimum Fe/Mo ratio exhibits NH_3 produc-

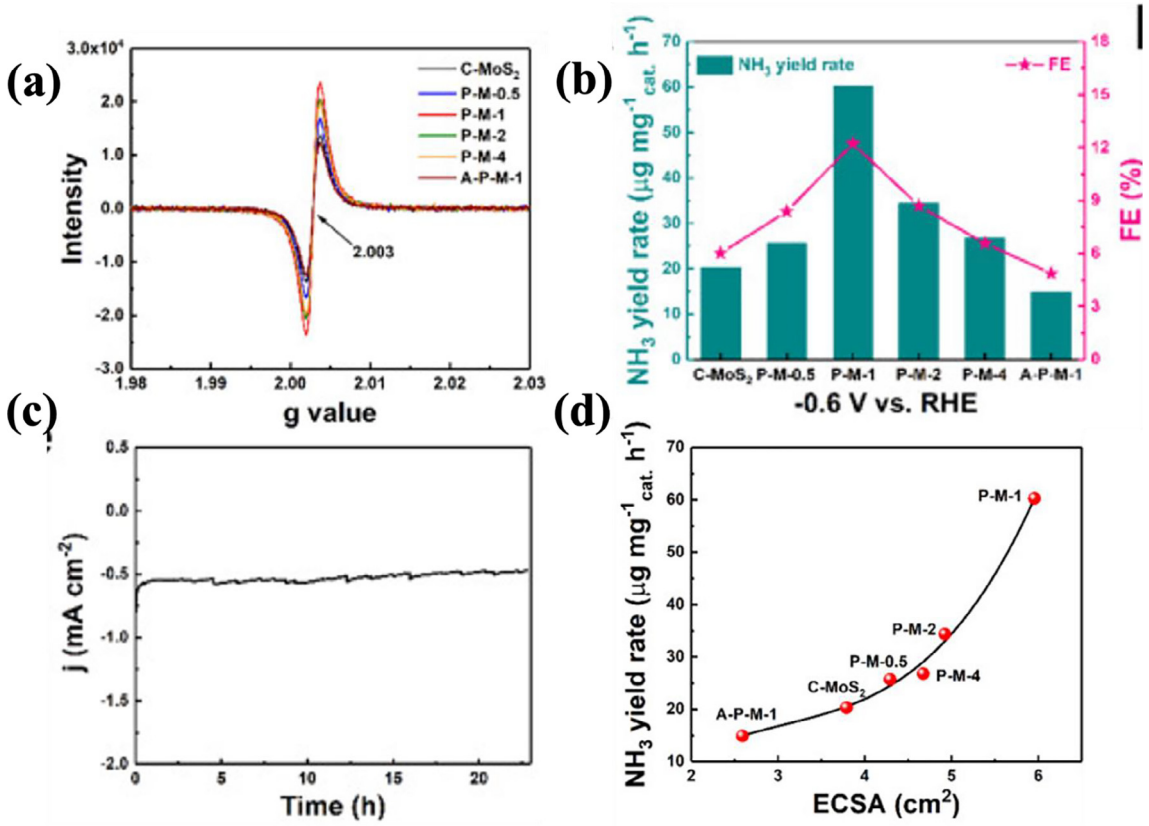

Fig. 12. (a) EPR spectra generated by the Mo-S dangling bonds for the different MoS_2 samples (b) Comparison NH_3 yield rates and FEs at −0.6 V vs RHE for various catalysts under the same conditions (c) Time-dependent current density curve of P-M−1 at −0.6 V for 23 h. (d) Evolution of the NH_3 yield rates with the value of ECSA. Reproduced with permission from [120]. Copyright 2021, Elsevier.

tion rate of 8.45 μg h^{-1} cm^{-2} and FE of 2.96 % in a pH neutral electrolyte at −0.5 V. This hybrid catalyst offers a promising NRR activity by imitating the natural FeMoS-nitrogenases. A similar study was reported by Yang and coworkers designing flower cluster-like FeS_2-MoS_2 hybrid catalyst employing a conductive 3D iron foam (IF) as a support and the iron source [125]. The prepared FeS_2-MoS_2@IF_{200} shows a significant NH_3 production rate of 7.1 × 10^{-10} mol s^{-1} cm^{-2} at −0.5 V and an optimal faradaic efficiency of 4.6 % at −0.3 V in 0.1 M KOH. This is a much higher performance compared to the single MoS_2 and FeS_2 counterparts.

In another effort to modulate interfacial charge distribution and promote N_2 adsorption, Yang et al. constructed CoS_2/MoS_2 nanocomposite catalyst with CoS_2 nanoparticles loaded on MoS_2 nanosheets and controlling the Mo/Co atomic ratios [126]. The composite catalyst displayed a superb NRR performance with a NH_3 production of 54.7 μg h^{-1} mg_{cat}^{-1} and an outstanding FE of 20.8 % in 0.1 M Li_2SO_4. The strong interfacial interaction between CoS_2 and MoS_2 in the composite, the N_2 binding and activation role of CoS_2 and MoS_2 acting as center for hydrogenation facilitated NH_3 formation.

Designing a multi-phased interface offers an opportunity to create more active catalytic sites and provide electron-transfer channels. Liu et al. prepared $FeNi_2S_4$/NiS hetero-interface electrocatalysts using NiFe-MOF-74 precursor supported on carbon cloth and investigated the effects of interfaces on the NRR activity [127]. By varying the Fe:Ni stoichiometric ratios, the morphology and exposed crystal planes of $FeNi_2S_4$/NiS were modulated, which helps in regulating the electronic structures. The optimized $FeNi_2S_4$/NiS electrocatalyst displayed an excellent NRR activity of 128.398 ± 1.32 μg h^{-1} cm^{-2} and a high FE of 28.64 ± 0.18 % at −0.30 V in 0.1 M KOH. The outstanding NRR activity can be ascribed to the formation of double-phase interface (DPI) with regulated exposed crystal planes and having a strong interaction. Zhang et al. synthesized Fe doped $Cu_{2-x}S$ quantum dots (QDs) by adding an Fe precursor during the synthesis of $Cu_{2-x}S$ [128]. It is demonstrated that by controlling the amount of Fe dopant, double-phased $Cu_{2-x}S$/Cu_5FeS_4 could be prepared. Combining the synergetic effect of the double-phase interface and Fe doping, the optimized $Cu_{2-x}S$/Cu_5FeS_4 QD displayed an NH_3 yield of 26.4 μg h^{-1} mg_{cat}^{-1} at −0.1 V and an FE of 3.1 % at −0.7 V in 0.1 M Na_2SO_4.

4.3.2. Metal/metal sulfide interface

A metal–semiconductor junction can modulate both the band positions of the semiconductor and the d-band center of the surface-active atoms [129,130]. It thus helps to lower the activation barrier of N_2 and suppress the competitive HER and hence improve the faradic efficiency.

Biswas et al. prepared NPG@SnS_2 by assembling hexagonal SnS_2 facets over a cubic nanoporous gold (NPG) layer [131]. The NPG@SnS_2 electrocatalyst attained one of the highest FE reported, as high as 49.3 % at −0.5 V in 0.1 M Na_2SO_4. The catalyst also displayed an excellent stability with no compromise in NRR activity for 22 h. The lower work function displayed by NPG@SnS_2 than SnS_2 and the adjusted d-band center of Sn atom resulted in the reduction of HER activity and a strikingly high FE. In another study, by taking advantage of the strong binding force between Au–S bonds, Zhou and coworkers developed AuNPs@MoS_2 by directly growing ultra-fine AuNPs on MoS_2 nanosheets [132]. The AuNPs@MoS_2 showed excellent NRR performance with an average NH_3 production rate of 25 mg h^{-1} mg_{cat}^{-1} and FE of 9.7 % at −0.3 V in 0.1 M KOH and demonstrated remarkable stability in all pH conditions. This high NRR performance is due to the strong interactions between AuNPs

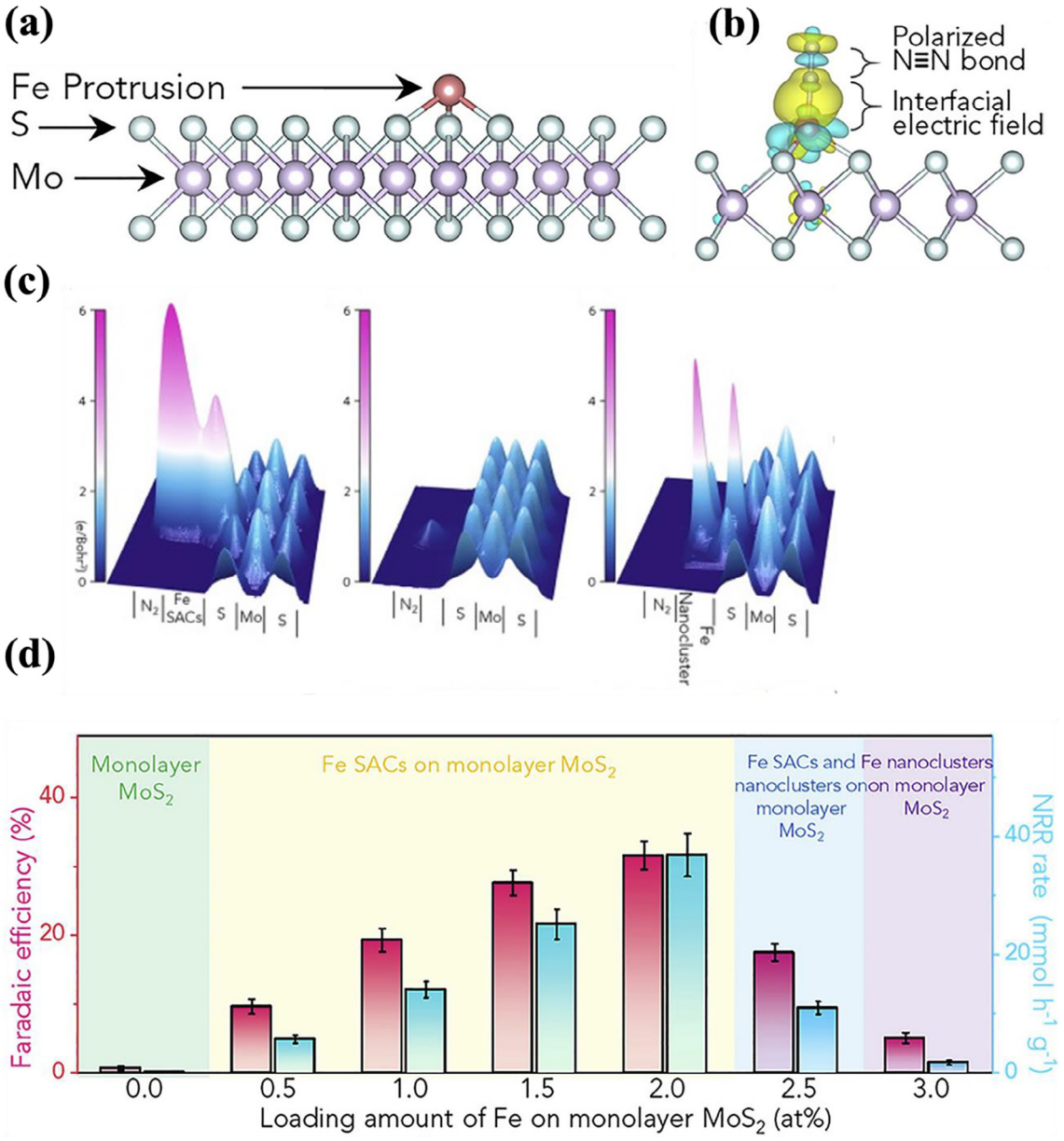

Fig. 13. (a) The protrusions formed by coordinating Fe-SA with three nearest neighboring S of Mo (b) Charge density differences of N_2 adsorbed onto Fe SAC protrusion immobilized on MoS_2 (c) 3D topographic potential distribution images of N2 adsorbed onto Fe SAC protrusion immobilized on MoS_2, pure MoS_2, and Fe nanocluster immobilized on MoS_2 (d) Performance comparison of SACs-MoS_2-Fe-Y (Y = 0.5, 1.0, 1.5, 2.0, 2.5, and 3.0 atom %) at 0.2 V versus RHE in flow cell. Reproduced with permission from [136]. Copyright 2020, Elsevier.

and MoS_2, the HER inhibiting effect of 2H MoS_2, and the synergistic effect of AuNPs and MoS_2.

Polymorph engineering of MoS_2 is an effective approach to inhibit HER kinetics to achieve high NRR performance and selectivity. To suppress the high HER activity of the metallic phase of 1T-MoS_2, Suryanto and co-workers designed Ru clusters decorated semiconductor phase 2H-MoS_2 (Ru/2H-MoS_2) [133]. The Ru/2H-MoS_2 displays NH_3 production rate of 6.7×10^{-11} mol cm^{-2} s^{-1} and high FE of 17.6 % in 0.01 M HCl at −0.2 V with NRR, which is 7 times more than that of Ru/1T-MoS_2. The Ru clusters were shown to be the active sites for adsorption of N_2 and the S vacancies in the 2H-MoS_2 bind the H^+. The high NRR performance and selectivity derives from the cumulative effect of introduction of active sites of Ru and the S-vacancies on the semiconducting 2H-MoS_2, which plays an important role in suppressing the HER.

Single-atom catalysts (SACs) are those that contain atomically dispersed sites anchored on supports and have received big interest as photocatalytic/electrocatalytic materials for nitrogen fixation [134]. They have the advantage of efficient atom utilization and outstanding catalytic activity and selectivity due to the suppressed HER [135]. Li and coworkers proposed a novel.

interfacial polarization strategy triggered by SACs supported on atomically thin MoS_2 nanosheets as an efficient approach to enhance N≡N cleavage [136]. They demonstrated that Fe single-atom catalysts with protrusion-shape supported onto the MoS_2 nanosheets (SACs-MoS_2-Fe) achieved a superior NH_3 yield rate of 36.1 ± 3.6 mmol g^{-1}-h^{-1} (97.5 ± 6 mg $h^{-1}cm^{-2}$) and FE of 31.6 % ± 2 % (Fig. 13). The NRR was carried out in a flow cell at −0.2 V in 0.1 M KCl. This NRR activity is 240-fold performance compared with monolayer MoS_2. The *in*-situ EXAFS, XANES and theoretical studies identified the Fe protru-

sion as the catalytically active center while the Mo and S act as the spectators during the NRR. Thus, the polarization triggered by curvature-rich surface of SAC protrusion and the heterojunction interface drives the superior NRR performance by enabling faster electron transfer and subsequent N_2 activation.

4.3.3. Metal sulfide/carbon interface

Owing to their enhanced electronic conductivity, high electrochemical active surface area and chemical stability, carbon-interfaced electrocatalysts have been explored as effective catalysts for NRR.

Designing 2D/2D hybrid materials using a carbon support to improve the contact interface has been used as an effective strategy to develop highly active electrocatalysts. Carbon nitrides, due to their unique 2D morphology and tunable electronic structure, have been considered as highly attractive carbon support for transition metal based electrocatalysts. Chu et al. reported a 2D/2D heterostructures of MoS_2/g-C_3N_4, in which the MoS_2 was grown in situ on g-C_3N_4 nanosheets with an improved interface [137]. The MoS_2/g-C_3N_4 heterostructure offered an enhanced NRR activity with a high FE of 17.8 % and an NH_3 yield of 18.5 μg h^{-1} mg^{-1} at −0.3 V in 0.1 M $LiClO_4$. The efficient contact interface between MoS_2 and g-C_3N_4 effectively improves the NRR performance by promoting the stabilization of *N_2H intermediate on Mo edges and simultaneously decreasing the energy barrier. It also hinders the competing HER on the Mo edge sites that are NRR-active.

Constructing bridging bonds at the interface to form a strongly coupled hybrid catalysts can effectively boost the NRR activity. Chen et al. synthesized CoS_x/NS-G hybrids by growing small cobalt sulfide nanoparticles on a graphene nanosheet (NS-G) and in situ annealing method [138]. Detailed characterizations by using XANES demonstrated that there exist bridging bonds of Co–N/S—C formed at the CoS_x-graphene interface allowing the charge transfer from Co to the NS-G. The CoS_2/NS-G hybrid exhibits superb NRR activity with NH_3 generation rate of 25.0 μg h^{-1} mg_{cat}^{-1} at −0.2 V and an outstanding FE of 25.9 % at −0.05 V. The result indicates that the interface created by the strong bridging bonds can accelerate transfer of electrons and improve the NRR. Wu et al. also reported strongly chemically coupled NiCoS/C nanocages prepared by etching the precursor ZIF-67 nanocubes and vulcanizing at low temperatures. Owing to the strong chemical interaction effects between C and NiCoS and unique nanocage structure, it attained a high NH_3 production of 26.0 μg h^{-1} mg^{-1} and FE of 12.9 % at 0 V in 0.1 M Li_2SO_4. The theoretical studies have shown that chemically coupled NiCoS/C adsorbs N_2 stronger than that of NiCoS and suppresses the hydrogen evolution reaction, resulting in enhanced NRR activity and selectivity.

4.4. Multi-site metal sulfides

Constructing catalysts with multiple active sites for synergistic N_2 adsorption and activation of key intermediates, can significantly accelerate N_2 fixation and inhibit the undesired HER [139,140]. The metalloenzymes such as MoFe nitrogenase in nature typically have both a N_2 binding protein and a reducing protein that provide sites that can synergistically assist N_2 adsorption and activation.

Lu and coworkers synthesized a bioinspired Fe-Mo-S based Chevrel phase chalcogenide $Fe_2Mo_6S_8$ as a selective electrocatalyst [141]. The unique structure of $Fe_2Mo_6S_8$ provides multiple active binding sites with the Fe/Mo sites for activating N_2 and the Fe-promoted S site for adsorbing reactive H_{ad}* intermediates (Fig. 14). A FE up to 12.5 % was observed at −0.20 V and a stable NH_3 yield rate of

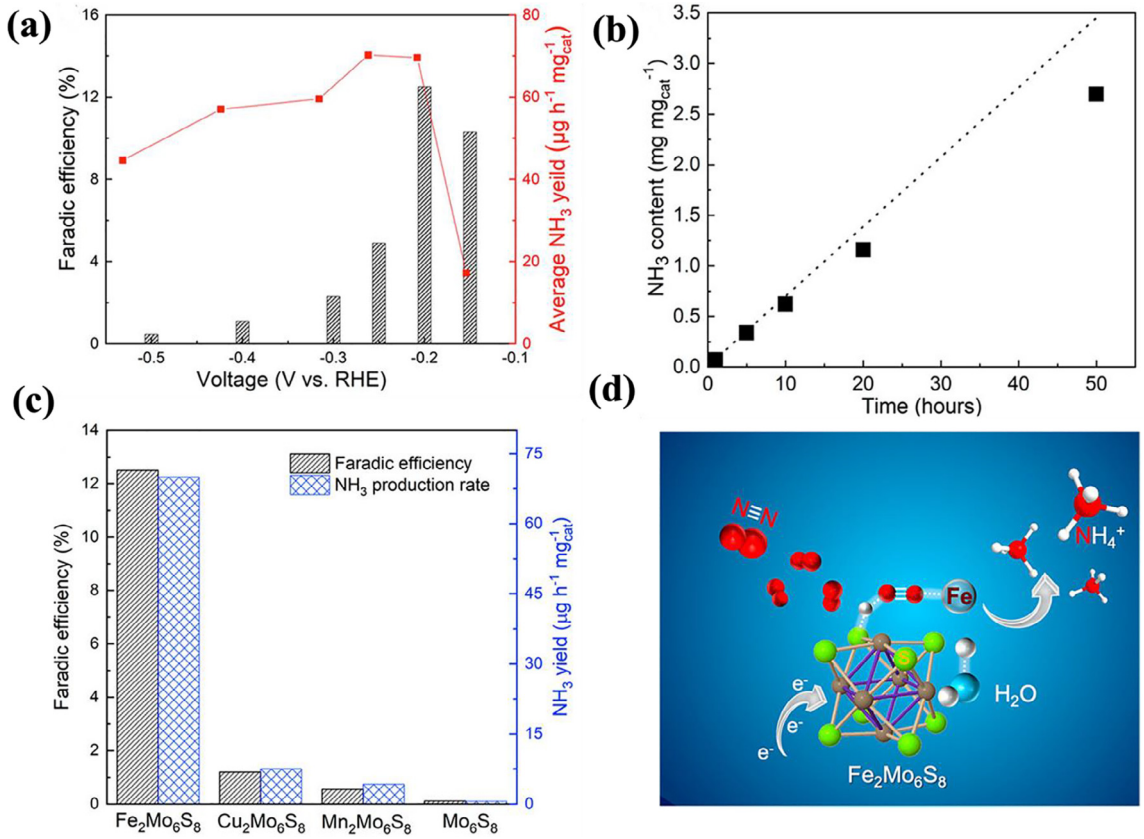

Fig. 14. (a) Comparison of Faradaic efficiency and corresponding NH_3 yield rates under different applied potential (b) Durability of the $Fe_2Mo_6S_8$ catalysts as revealed from the relationship between ammonia content and electrolysis duration for 50 h (at −0.2 V) (c) Comparison of N_2 to NH_3 conversion efficiency and average NH_3 production rate for Mo_6S_8 and $M_2Mo_6S_8$ (M = Fe, Mn, and Cu) electrocatalysts and (d) Schematic illustration of the proposed binding mechanism for N_2 absorption and subsequent conversion to NH_3. Reproduced with permission from [141]. Copyright 2021, American Chemical Society.

70 μg h^{-1} mg_{cat}^{-1} in 0.5 M Na_2SO_4 and 0.1 M sodium citrate buffer for 50 h. The comparative activity of the same Chevrel phase structures but different modulator cations including Mo_6S_8, $Cu_2Mo_6S_8$, and Mn_2-Mo_6S_8 exhibited much lower N_2 conversion activity. It was demonstrated that the interactions between Fe and Mo_6S_8 clusters modulate the catalytic pathways, and the Fe plays important roles by involving in the absorption and/or conversion of N_2.

Modulating and understanding the intermediates that form on the surface of an electrocatalyst during NRR is vital to overcome limitations associated with the adsorption of N_2 molecules. Fu *et al.* constructed an intermetallic ternary Re_2MnS_6 nanosheets with hybridized dual-metal Mn-Re sites to efficiently activate N_2 [142]. A FE of 17.42 % and NH_3 yield rate of 3.78 μg h^{-1} mg_{cat}^{-1} was obtained at −0.2 V and −0.3 V, respectively in 0.1 M Na_2SO_4. This NH_3 yield rate is 6.6-fold more than that of the ReS_2. The dual-metal sites allow the simultaneous bonding of both N atoms of N_2 molecule to form a more stable intermediate Re—N—N—Mn in the alternating process. This strategy interrupts the limitations associated with the distal pathway on a single metal site and effectively improves N_2 reduction into NH_3.

5. Conclusions and perspectives

Photocatalytic and electrocatalytic nitrogen fixation to ammonia is considered as a sustainable and green alternative to the traditional Haber–Bosch process owing to the use of renewable energy to drive the processes. Compared with photocatalysis, the electrocatalytic NRR is more efficient because of the inadequate utilization of photons with photocatalysts. However, if the photocatalytic technology can achieve a high solar-to-fuel conversion efficiency, it would become a preferable process. These processes, however, require innovative advances in the design of efficient catalysts to make them favorable technologies for artificial ammonia production. Metal sulfides have recently attracted a great attention as effective and efficient electrocatalysts and photocatalysts for nitrogen fixation due to their structural similarity to the active site of the nitrogenase, presence of rich active sites, adjustable electronic properties, and relatively narrow bandgaps. Various metal sulfide-based catalysts have been investigated for artificial fixation of nitrogen. Considering the diversity of metal sulfides there is more to explore further about this class of catalysts as efficient and effective catalytic materials for artificial nitrogen fixation. Here, this review outlines the latest advances in transition metal sulfide-based photocatalysts and electrocatalysts for nitrogen fixation to ammonia at ambient conditions. The focus of this review is on the various modification strategies to introduce more active sites for N_2 activation and thus to improve the overall activity of the nitrogen fixation on metal sulfides.

i) Metal sulfide based photocatalysts have appropriate band gap and can absorb visible light making them suitable for nitrogen fixation. However, studies carried out so far over metal sulfides are limited, mainly based on CdS, and they display poor efficiency. There are various metal sulfides such as 2D metal disulfides (MX_2; M = Mo, W, Re & X = S, Se), ternary zinc indium sulfides (Zn-In-S), that are theoretically and experimentally predicted to be potentially active for catalytic nitrogen fixation [59]. The key to make use of these and other new class of metal sulfide based materials as effective photocatalysts lies in developing different modifications strategies that can create more active sites on the metal and sulfur edges [103]. This includes creating defect, morphology control, doping, and employing co-catalysts. These modifications will enhance the nitrogen adsorption and activation, light absorption and charge separation and thus boost the photocatalytic performance. The easy active site modification of metal sulfides can benefit in widening the range of photocatalytic material types, properties and N_2 activation mechanisms.
ii) Considerable progress has been made on exploration of metal sulfides for electrocatalytic nitrogen fixation. However, sufficient faradaic efficiency has not been achieved yet. The electrocatalytic activity of metal sulfides can be improved by regulating their electronic structure through defect and interface engineering. In addition, several strategies have been employed to suppress the HER and enhance the efficiency and selectivity of the NRR. New types of multisite metal sulfides, which mimic the metalloenzyme nitrogenase, are currently being investigated displaying a significantly enhanced NRR activity and provide more insight into the mechanism of N_2 fixation.
iii) Although there are promising developments in the design of catalysts and overall improvement of the nitrogen fixation process, the catalytic efficiency and the amount of ammonia produced are still very low. This leads to possible experimental errors impeding the reliable analysis of produced ammonia. This is one of the main challenges that needs to be addressed in a more convincing approach. The determination of ammonia produced needs a rigorous experimental methodology to avoid any false positives originating from different sources of contamination and to make reliable conclusion. Proper blank experiments need to be carried out to exclude the ammonia from the background. Colorimetric method, as the most common ammonia quantification technique, needs to be complemented by other methods such as ion chromatography, NMR spectroscopic techniques, and isotope labeled experiments.
iv) The deep understanding of the reaction mechanisms is important to have the overall picture of the nitrogen fixation process and helps in devising better ways of catalyst design. Advanced theoretical calculations and experimental methods such as in-situ studies should be applied to explore the detailed processes and investigate intermediates. Thus, with more concerted efforts among the scientific community a breakthrough could be achieved for artificial nitrogen fixation in the near future using novel catalytic materials including metal sulfides.

Data availability

No data was used for the research described in the article.

Declaration of Competing Interest

The authors declare that they have no known competing financial interests or personal relationships that could have appeared to influence the work reported in this paper.

Acknowledgements

University of Trieste (project FRA 2021), Ministry of University and Research, INSTM Consortium and ICCOM-CNR are acknowledged for financial support.

References

[1] V. Rosca, M. Duca, M.T. de Groot, M.T.M. Koper, Nitrogen cycle electrocatalysis, Chem. Rev. 109 (2009) 2209–2244, https://doi.org/10.1021/cr8003696.
[2] D.E. Canfield, A.N. Glazer, P.G. Falkowski, The evolution and future of Earth's nitrogen cycle, Science 330 (6001) (2010) 192–196.
[3] B. Thamdrup, New pathways and processes in the global nitrogen cycle, Annu. Rev. Ecol. Evol. Syst. 43 (2012) 407–428, https://doi.org/10.1146/annurev-ecolsys-102710-145048.
[4] B.K. Burgess, D.J. Lowe, Mechanism of molybdenum nitrogenase, Chem. Rev. 96 (1996) 2983–3012, https://doi.org/10.1021/cr950055x.

[5] B.M. Hoffman, D. Lukoyanov, Z.-Y. Yang, D.R. Dean, L.C. Seefeldt, Mechanism of nitrogen fixation by nitrogenase: the next stage, Chem. Rev. 114 (8) (2014) 4041–4062.

[6] T. Spatzal, M. Aksoyoglu, L. Zhang, S.L. Andrade, E. Schleicher, S. Weber, D.C. Rees, O. Einsle, Evidence for interstitial carbon in nitrogenase FeMo cofactor, Science 334 (2011) 940.

[7] K. Danyal, D.R. Dean, B.M. Hoffman, L.C. Seefeldt, Electron transfer within nitrogenase: evidence for a deficit-spending mechanism, Biochemistry. 50 (2011) 9255–9263.

[8] B.M. Hoffman, D.R. Dean, L.C. Seefeldt, Climbing nitrogenase: toward a mechanism of enzymatic nitrogen fixation, Acc. Chem. Res. 42 (2009) 609–619, https://doi.org/10.1021/ar8002128.

[9] S. Raugei, L.C. Seefeldt, B.M. Hoffman, Critical computational analysis illuminates the reductive-elimination mechanism that activates nitrogenase for N2 reduction, Proc. Natl. Acad. Sci. 115 (2018) E10521–E10530.

[10] K.C. MacLeod, P.L. Holland, Recent developments in the homogeneous reduction of dinitrogen by molybdenum and iron, Nat. Chem. 5 (2013) 559–565, https://doi.org/10.1038/nchem.1620.

[11] T. Rayment, R. Schlögl, J.M. Thomas, G. Ertl, Structure of the ammonia synthesis catalyst, Nature. 315 (6017) (1985) 311–313.

[12] R. Raja, G. Sankar, J.M. Thomas, Bifunctional molecular sieve catalysts for the benign ammoximation of cyclohexanone: one-step, solvent-free production of oxime and ε-caprolactam with a mixture of air and ammonia, J. Am. Chem. Soc. 123 (2001) 8153–8154, https://doi.org/10.1021/ja011001+.

[13] W. Zhao, H. Xi, M. Zhang, Y. Li, J. Chen, J. Zhang, X. Zhu, Enhanced quantum yield of nitrogen fixation for hydrogen storage with in situ-formed carbonaceous radicals, Chem. Commun. 51 (2015) 4785–4788, https://doi.org/10.1039/C5CC00589B.

[14] A. Scott, Ammonia en route to fuel ships and planes, Chem. Eng. News. 98 (2020) 12.

[15] V. Smil, Detonator of the population explosion, Nature 400 (1999) 415, https://doi.org/10.1038/22672.

[16] N. Hazari, Homogeneous iron complexes for the conversion of dinitrogen into ammonia and hydrazine, Chem. Soc. Rev. 39 (2010) 4044–4056, https://doi.org/10.1039/B919680N.

[17] H. Liu, Ammonia synthesis catalyst 100 years: practice, enlightenment and challenge, Chin. J. Catal. 35 (2014) 1619–1640, https://doi.org/10.1016/S1872-2067(14)60118-2.

[18] R. Shi, X. Zhang, G.I. Waterhouse, Y. Zhao, T. Zhang, The journey toward low temperature, low pressure catalytic nitrogen fixation, Adv. Energy Mater. 10 (2020) 2000659.

[19] R. Li, Photocatalytic nitrogen fixation: an attractive approach for artificial photocatalysis, Chin. J. Catal. 39 (2018) 1180–1188, https://doi.org/10.1016/S1872-2067(18)63104-3.

[20] G. Soloveichik, Electrochemical synthesis of ammonia as a potential alternative to the Haber-Bosch process, Nat. Catal. 2 (5) (2019) 377–380.

[21] C. Mao, L. Yu, J. Li, J. Zhao, L. Zhang, Energy-confined solar thermal ammonia synthesis with K/Ru/TiO_2-xHx, Appl. Catal. B Environ. 224 (2018) 612–620, https://doi.org/10.1016/j.apcatb.2017.11.010.

[22] L.R. Winter, J.G. Chen, N_2 Fixation by plasma-activated processes, Joule. 5 (2021) 300–315, https://doi.org/10.1016/j.joule.2020.11.009.

[23] B.S. Patil, Q. Wang, V. Hessel, J. Lang, Plasma N_2-fixation: 1900–2014, Catal. Today 256 (2015) 49–66, https://doi.org/10.1016/j.cattod.2015.05.005.

[24] K. Ithisuphalap, H. Zhang, L. Guo, Q. Yang, H. Yang, G. Wu, Photocatalysis and photoelectrocatalysis methods of nitrogen reduction for sustainable ammonia synthesis, Small Methods 3 (2019) 1800352.

[25] X. Chen, N. Li, Z. Kong, W.-J. Ong, X. Zhao, Photocatalytic fixation of nitrogen to ammonia: state-of-the-art advancements and future prospects, Mater. Horiz. 5 (2018) 9–27.

[26] D. Chanda, R. Xing, T. Xu, Q. Liu, Y. Luo, S. Liu, R.A. Tufa, T.H. Dolla, T. Montini, X. Sun, Electrochemical nitrogen reduction: recent progress and prospects, Chem. Commun. 57 (2021) 7335–7349, https://doi.org/10.1039/D1CC01451J.

[27] B. Yang, W. Ding, H. Zhang, S. Zhang, Recent progress in electrochemical synthesis of ammonia from nitrogen: strategies to improve the catalytic activity and selectivity, Energy Environ. Sci. 14 (2021) 672–687.

[28] K. Tanifuji, Y. Ohki, Metal–sulfur compounds in N_2 reduction and nitrogenase-related chemistry, Chem. Rev. 120 (12) (2020) 5194–5251.

[29] Y. Roux, C. Duboc, M. Gennari, Molecular catalysts for N_2 reduction: state of the art, mechanism, and challenges, ChemPhysChem 18 (2017) 2606–2617.

[30] S. Sun, X. Li, W. Wang, L. Zhang, X. Sun, Photocatalytic robust solar energy reduction of dinitrogen to ammonia on ultrathin MoS_2, Appl. Catal. B Environ. 200 (2017) 323–329, https://doi.org/10.1016/j.apcatb.2016.07.025.

[31] A. Kudo, Y. Miseki, Heterogeneous photocatalyst materials for water splitting, Chem. Soc. Rev. 38 (2009) 253–278, https://doi.org/10.1039/B800489G.

[32] X. Gao, L. An, D. Qu, W. Jiang, Y. Chai, S. Sun, X. Liu, Z. Sun, Enhanced photocatalytic N_2 fixation by promoting N_2 adsorption with a co-catalyst, Sci. Bull. 64 (2019) 918–925, https://doi.org/10.1016/j.scib.2019.05.009.

[33] Z. He, Y. Wang, X. Dong, N. Zheng, H. Ma, X. Zhang, Indium sulfide nanotubes with sulfur vacancies as an efficient photocatalyst for nitrogen fixation, RSC Adv. 9 (2019) 21646–21652, https://doi.org/10.1039/C9RA03507A.

[34] X. Tong, M. Benyuan, L. Jie, Y. Luchao, L. Qian, L. Tingshuai, Z. Haitao, L. Yonglan, L. Siyu, S. Xuping, Recent progress in metal-free electrocatalysts toward ambient N 2 reduction reaction, Acta Phys.-Chim. Sin. 37 (2021) 2009043.

[35] X. Chen, S. Zhang, X. Qian, Z. Liang, Y. Xue, X. Zhang, J. Tian, Y. Han, M. Shao, Enabling efficient electrocatalytic conversion of N_2 to NH_3 by Ti_3C_2 MXene loaded with semi-metallic 1T′-MoS_2 nanosheets, Appl. Catal. B Environ. 310 (2022) 121277.

[36] X. Chen, C. Ma, Z. Tan, X. Wang, X. Qian, X. Zhang, J. Tian, S. Yan, M. Shao, One-dimensional screw-like MoS_2 with oxygen partially replacing sulfur as an electrocatalyst for the N_2 reduction reaction, Chem. Eng. J. 433 (2022), https://doi.org/10.1016/j.cej.2022.134504 134504.

[37] A. Hellman, E.J. Baerends, M. Biczysko, T. Bligaard, C.H. Christensen, D.C. Clary, S. Dahl, R. van Harrevelt, K. Honkala, H. Jonsson, G.J. Kroes, M. Luppi, U. Manthe, J.K. Nørskov, R.A. Olsen, J. Rossmeisl, E. Skúlason, C.S. Tautermann, A. J.C. Varandas, J.K. Vincent, Predicting catalysis: understanding ammonia synthesis from first-principles calculations, J. Phys. Chem. B. 110 (2006) 17719–17735, https://doi.org/10.1021/jp056982h.

[38] D. Hao, Y. Liu, S. Gao, H. Arandiyan, X. Bai, Q. Kong, W. Wei, P.K. Shen, B.-J. Ni, Emerging artificial nitrogen cycle processes through novel electrochemical and photochemical synthesis, Mater. Today. 46 (2021) 212–233, https://doi.org/10.1016/j.mattod.2021.01.029.

[39] D. Lukoyanov, S.A. Dikanov, Z.-Y. Yang, B.M. Barney, R.I. Samoilova, K.V. Narasimhulu, D.R. Dean, L.C. Seefeldt, B.M. Hoffman, ENDOR/HYSCORE studies of the common intermediate trapped during nitrogenase reduction of N_2H_2, CH_3N_2H, and N_2H_4 support an alternating reaction pathway for N_2 reduction, J. Am. Chem. Soc. 133 (30) (2011) 11655–11664.

[40] G.N. Schrauzer, T.D. Guth, Photolysis of water and photoreduction of nitrogen on titanium dioxide, J. Am. Chem. Soc. 99 (1977) 7189–7193, https://doi.org/10.1021/ja00464a015.

[41] T. Hisatomi, J. Kubota, K. Domen, Recent advances in semiconductors for photocatalytic and photoelectrochemical water splitting, Chem. Soc. Rev. 43 (2014) 7520–7535, https://doi.org/10.1039/C3CS60378D.

[42] X. Chang, T. Wang, J. Gong, CO_2 photo-reduction: insights into CO_2 activation and reaction on surfaces of photocatalysts, Energy Environ. Sci. 9 (2016) 2177–2196, https://doi.org/10.1039/C6EE00383D.

[43] H. Shen, M. Yang, L. Hao, J. Wang, J. Strunk, Z. Sun, Photocatalytic nitrogen reduction to ammonia: insights into the role of defect engineering in photocatalysts, Nano Res. (2021) 1–37.

[44] G. Chen, D. Li, F. Li, Y. Fan, H. Zhao, Y. Luo, R. Yu, Q. Meng, Ball-milling combined calcination synthesis of MoS_2/CdS photocatalysts for high photocatalytic H_2 evolution activity under visible light irradiation, Appl. Catal. Gen. 443–444 (2012) 138–144, https://doi.org/10.1016/j.apcata.2012.07.033.

[45] H. Huang, B. Dai, W. Wang, C. Lu, J. Kou, Y. Ni, L. Wang, Z. Xu, Oriented built-in electric field introduced by surface gradient diffusion doping for enhanced photocatalytic H_2 evolution in CdS nanorods, Nano Lett. 17 (2017) 3803–3808, https://doi.org/10.1021/acs.nanolett.7b01147.

[46] D. Ma, J.-W. Shi, Y. Zou, Z. Fan, X. Ji, C. Niu, Highly efficient photocatalyst based on a CdS quantum dots/ZnO Nanosheets 0D/2D heterojunction for hydrogen evolution from water splitting, ACS Appl. Mater. Interfaces 9 (2017) 25377–25386, https://doi.org/10.1021/acsami.7b08407.

[47] Y. Li, H. Wang, S. Peng, Tunable photodeposition of MoS_2 onto a composite of reduced graphene oxide and CdS for synergic photocatalytic hydrogen generation, J. Phys. Chem. C. 118 (2014) 19842–19848, https://doi.org/10.1021/jp5054474.

[48] Y. Hu, X. Gao, L. Yu, Y. Wang, J. Ning, S. Xu, X.W. (David) Lou, Carbon-coated CdS petalous nanostructures with enhanced photostability and photocatalytic activity, Angew. Chem. Int. Ed. 52 (2013) 5636–5639. 10.1002/anie.201301709.

[49] W. Dong, Y. Liu, G. Zeng, T. Cai, L. Shao, H. Chen, W. Zeng, X. Xia, Crystal phase engineering $Zn_{0.8}Cd_{0.2}S$ nanocrystals with twin-induced homojunctions for photocatalytic nitrogen fixation under visible light, J. Photochem. Photobiol. Chem. 401 (2020), https://doi.org/10.1016/j.jphotochem.2020.112766 112766.

[50] L. Ye, C. Han, Z. Ma, Y. Leng, J. Li, X. Ji, D. Bi, H. Xie, Z. Huang, Ni_2P loading on $Cd_{0.5}Zn_{0.5}S$ solid solution for exceptional photocatalytic nitrogen fixation under visible light, Chem. Eng. J. 307 (2017) 311–318, https://doi.org/10.1016/j.cej.2016.08.102.

[51] Z.-K. Shen, Y.-J. Yuan, P. Wang, W. Bai, L. Pei, S. Wu, Z.-T. Yu, Z. Zou, Few-layer black phosphorus nanosheets: a metal-free cocatalyst for photocatalytic nitrogen fixation, ACS Appl. Mater. Interfaces 12 (2020) 17343–17352, https://doi.org/10.1021/acsami.9b21167.

[52] B. Sun, Z. Liang, Y. Qian, X. Xu, Y. Han, J. Tian, Sulfur vacancy-rich O-doped 1T-MoS_2 nanosheets for exceptional photocatalytic nitrogen fixation over CdS, ACS Appl. Mater. Interfaces 12 (2020) 7257–7269, https://doi.org/10.1021/acsami.9b20767.

[53] R. Shi, Y. Zhao, G.I.N. Waterhouse, S. Zhang, T. Zhang, Defect engineering in photocatalytic nitrogen fixation, ACS Catal. 9 (2019) 9739–9750, https://doi.org/10.1021/acscatal.9b03246.

[54] C. Mao, J. Wang, Y. Zou, H. Li, G. Zhan, J. Li, J. Zhao, L. Zhang, Anion (O, N, C, and S) vacancies promoted photocatalytic nitrogen fixation, Green Chem. 21 (2019) 2852–2867, https://doi.org/10.1039/C9GC01010F.

[55] Y. Cao, S. Hu, F. Li, Z. Fan, J. Bai, G. Lu, Q. Wang, Photofixation of atmospheric nitrogen to ammonia with a novel ternary metal sulfide catalyst under visible light, RSC Adv. 6 (2016) 49862–49867, https://doi.org/10.1039/C6RA08247E.

[56] S. Hu, X. Chen, Q. Li, Y. Zhao, W. Mao, Effect of sulfur vacancies on the nitrogen photofixation performance of ternary metal sulfide photocatalysts, Catal, Sci. Technol. 6 (2016) 5884–5890, https://doi.org/10.1039/C6CY00622A.

[57] Z. Li, N.H. Attanayake, J.L. Blackburn, E.M. Miller, Carbon dioxide and nitrogen reduction reactions using 2D transition metal dichalcogenide (TMDC) and carbide/nitride (MXene) catalysts, Energy Environ. Sci. 14 (2021) 6242–6286, https://doi.org/10.1039/D1EE03211A.

[58] G. Giuffredi, T. Asset, Y. Liu, P. Atanassov, F. Di Fonzo, Transition metal chalcogenides as a versatile and tunable platform for catalytic CO_2 and N_2 electroreduction, ACS Mater. Au. 1 (2021) 6–36, https://doi.org/10.1021/acsmaterialsau.1c00006.

[59] F. Li, L. Chen, H. Liu, D. Wang, C. Shi, H. Pan, Enhanced N_2-fixation by engineering the edges of two-dimensional transition-metal disulfides, J. Phys. Chem. C. 123 (2019) 22221–22227, https://doi.org/10.1021/acs.jpcc.9b04730.

[60] X. Li, T. Li, Y. Ma, Q. Wei, W. Qiu, H. Guo, X. Shi, P. Zhang, A.M. Asiri, L. Chen, B. Tang, X. Sun, Boosted electrocatalytic N_2 reduction to NH_3 by defect-rich MoS_2 nanoflower, Adv. Energy Mater. 8 (2018) 1801357, https://doi.org/10.1002/aenm.201801357.

[61] L. Zhang, X. Ji, X. Ren, Y. Ma, X. Shi, Z. Tian, A.M. Asiri, L. Chen, B. Tang, X. Sun, Electrochemical ammonia synthesis via nitrogen reduction reaction on a MoS_2 catalyst: theoretical and experimental studies, Adv. Mater. 30 (2018) 1800191, https://doi.org/10.1002/adma.201800191.

[62] C. Lui, A. Frenzel, D. Pilon, Y.-H. Lee, X. Ling, G. Akselrod, J. Kong, N. Gedik, Trion-induced negative photoconductivity in monolayer MoS_2, Phys. Rev. Lett. 113 (2014) 166801.

[63] H. Chen, X. Wen, J. Zhang, T. Wu, Y. Gong, X. Zhang, J. Yuan, C. Yi, J. Lou, P.M. Ajayan, W. Zhuang, G. Zhang, J. Zheng, Ultrafast formation of interlayer hot excitons in atomically thin MoS_2/WS_2 heterostructures, Nat. Commun. 7 (2016) 12512, https://doi.org/10.1038/ncomms12512.

[64] B. Hu, B.-H. Wang, Z. Bai, L. Chen, J.-K. Guo, S. Shen, T.-L. Xie, C.-T. Au, L.-L. Jiang, S.-F. Yin, Regulating MoS_2 edge site for photocatalytic nitrogen fixation: a theoretical and experimental study, Chem. Eng. J. 442 (2022), https://doi.org/10.1016/j.cej.2022.136211 136211.

[65] R. Peng, L. Liang, Z.D. Hood, A. Boulesbaa, A. Puretzky, A.V. Ievlev, J. Come, O.S. Ovchinnikova, H. Wang, C. Ma, M. Chi, B.G. Sumpter, Z. Wu, In-plane heterojunctions enable multiphasic two-dimensional (2D) MoS_2 nanosheets as efficient photocatalysts for hydrogen evolution from water reduction, ACS Catal. 6 (2016) 6723–6729, https://doi.org/10.1021/acscatal.6b02076.

[66] D. Wang, X. Zhang, S. Bao, Z. Zhang, H. Fei, Z. Wu, Phase engineering of a multiphasic 1T/2H MoS_2 catalyst for highly efficient hydrogen evolution, J. Mater. Chem. A. 5 (2017) 2681–2688, https://doi.org/10.1039/C6TA09409K.

[67] J. Qin, W. Zhao, X. Hu, J. Li, P. Ndokoye, B. Liu, Exploring the N_2 adsorption and activation mechanisms over the 2H/1T mixed-phase ultrathin Mo1−xWxS2 nanosheets for boosting N_2 photosynthesis, ACS Appl. Mater. Interfaces. 13 (2021) 7127–7134, https://doi.org/10.1021/acsami.0c19282.

[68] H. Maimaitizi, A. Abulizi, T. Zhang, K. Okitsu, J. Zhu, Facile photo-ultrasonic assisted synthesis of flower-like Pt/N-MoS_2 microsphere as an efficient sonophotocatalyst for nitrogen fixation, Ultrason. Sonochem. 63 (2020), https://doi.org/10.1016/j.ultsonch.2019.104956 104956.

[69] L. Shi, Z. Li, L. Ju, A. Carrasco-Pena, N. Orlovskaya, H. Zhou, Y. Yang, Promoting nitrogen photofixation over a periodic WS2@TiO_2 nanoporous film, J. Mater. Chem. A. 8 (2020) 1059–1065, https://doi.org/10.1039/C9TA12743G.

[70] J. Zhang, H. Wang, X. Yuan, G. Zeng, W. Tu, S. Wang, Tailored indium sulfide-based materials for solar-energy conversion and utilization, J. Photochem. Photobiol. C Photochem. Rev. 38 (2019) 1–26, https://doi.org/10.1016/j.jphotochemrev.2018.11.001.

[71] X. Fu, X. Wang, Z. Chen, Z. Zhang, Z. Li, D.Y.C. Leung, L. Wu, X. Fu, Photocatalytic performance of tetragonal and cubic β-In2S3 for the water splitting under visible light irradiation, Appl. Catal. B Environ. 95 (2010) 393–399, https://doi.org/10.1016/j.apcatb.2010.01.018.

[72] W. Hou, Y. Xiao, G. Han, An interconnected ternary MIn_2S_4 (M = Fe Co, Ni) thiospinel nanosheet array: a type of efficient platinum-free counter electrode for dye-sensitized solar cells, Angew. Chem. Int. Ed. 56 (2017) 9146–9150, https://doi.org/10.1002/anie.201705399.

[73] S. Wang, B.Y. Guan, Y. Lu, X.w. "David" Lou, Formation of hierarchical In2S3–CdIn2S4 heterostructured nanotubes for efficient and stable visible light CO_2 reduction, J. Am. Chem. Soc. 139 (2017) 17305–17308, https://doi.org/10.1021/jacs.7b10733.

[74] J. Hou, S. Cao, Y. Sun, Y. Wu, F. Liang, Z. Lin, L. Sun, Water splitting: atomically thin mesoporous In2O3–x/In2S3 lateral heterostructures enabling robust broadband-light photo-electrochemical water splitting (Adv. Energy Mater. 9/2018), Adv. Energy Mater. 8 (2018) 1870040. 10.1002/aenm.201870040.

[75] B. Ma, M. Yue, P. Zhang, S. Li, R. Cong, W. Gao, T. Yang, Tetragonal β-In2S3: Partial ordering of In3+ vacancy and visible-light photocatalytic activities in both water and nitrate reduction, Catal. Commun. 88 (2017) 18–21, https://doi.org/10.1016/j.catcom.2016.09.029.

[76] H. Xu, Y. Wang, X. Dong, N. Zheng, H. Ma, X. Zhang, Fabrication of In2O3/In2S3 microsphere heterostructures for efficient and stable photocatalytic nitrogen fixation, Appl. Catal. B Environ. 257 (2019), https://doi.org/10.1016/j.apcatb.2019.117932 117932.

[77] S. Ding, X. Liu, Y. Shi, Y. Liu, T. Zhou, Z. Guo, J. Hu, Generalized synthesis of ternary sulfide hollow structures with enhanced photocatalytic performance for degradation and hydrogen evolution, ACS Appl. Mater. Interfaces 10 (2018) 17911–17922, https://doi.org/10.1021/acsami.8b02955.

[78] C. Du, Q. Zhang, Z. Lin, B. Yan, C. Xia, G. Yang, Half-unit-cell ZnIn2S4 monolayer with sulfur vacancies for photocatalytic hydrogen evolution, Appl. Catal. B Environ. 248 (2019) 193–201, https://doi.org/10.1016/j.apcatb.2019.02.027.

[79] X. Jiao, Z. Chen, X. Li, Y. Sun, S. Gao, W. Yan, C. Wang, Q. Zhang, Y. Lin, Y. Luo, Y. Xie, Defect-mediated electron-hole separation in one-unit-cell ZnIn2S4 layers for boosted solar-driven CO_2 reduction, J. Am. Chem. Soc. 139 (2017) 7586–7594, https://doi.org/10.1021/jacs.7b02290.

[80] N. Luo, T. Montini, J. Zhang, P. Fornasiero, E. Fonda, T. Hou, W. Nie, J. Lu, J. Liu, M. Heggen, L. Lin, C. Ma, M. Wang, F. Fan, S. Jin, F. Wang, Visible-light-driven coproduction of diesel precursors and hydrogen from lignocellulose-derived methylfurans, Nat. Energy 4 (2019) 575–584, https://doi.org/10.1038/s41560-019-0403-5.

[81] G. Han, X. Liu, Z. Cao, Y. Sun, Photocatalytic pinacol C-C coupling and jet fuel precursor production on ZnIn2S4 nanosheets, ACS Catal. 10 (2020) 9346–9355, https://doi.org/10.1021/acscatal.0c01715.

[82] W. Yang, L. Zhang, J. Xie, X. Zhang, Q. Liu, T. Yao, S. Wei, Q. Zhang, Y. Xie, Enhanced photoexcited carrier separation in oxygen-doped ZnIn2S4 nanosheets for hydrogen evolution, Angew. Chem. Int. Ed. 55 (2016) 6716–6720, https://doi.org/10.1002/anie.201602543.

[83] Y. Pan, X. Yuan, L. Jiang, H. Yu, J. Zhang, H. Wang, R. Guan, G. Zeng, Recent advances in synthesis, modification and photocatalytic applications of micro/nano-structured zinc indium sulfide, Chem. Eng. J. 354 (2018) 407–431, https://doi.org/10.1016/j.cej.2018.08.028.

[84] H. Han, Y. Yang, J. Liu, X. Zheng, X. Wang, S. Meng, S. Zhang, X. Fu, S. Chen, Effect of Zn vacancies in Zn3In2S6 nanosheets on boosting photocatalytic N_2 fixation, ACS Appl. Energy Mater. 3 (11) (2020) 11275–11284.

[85] G. Swain, S. Sultana, K. Parida, Constructing a novel surfactant-free MoS_2 nanosheet modified MgIn2S4 marigold microflower: an efficient visible-light driven 2D–2D p-n heterojunction photocatalyst toward HER and pH regulated NRR, ACS Sustain. Chem. Eng. 8 (2020) 4848–4862, https://doi.org/10.1021/acssuschemeng.9b07821.

[86] J. Lee, L.-L. Tan, S.-P. Chai, Heterojunction photocatalysts for artificial nitrogen fixation: fundamentals, latest advances and future perspectives, Nanoscale 13 (2021) 7011–7033, https://doi.org/10.1039/D1NR00783A.

[87] H. Wang, L. Zhang, Z. Chen, J. Hu, S. Li, Z. Wang, J. Liu, X. Wang, Semiconductor heterojunction photocatalysts: design, construction, and photocatalytic performances, Chem. Soc. Rev. 43 (2014) 5234–5244, https://doi.org/10.1039/C4CS00126E.

[88] Q. Zhang, S. Hu, Z. Fan, D. Liu, Y. Zhao, H. Ma, F. Li, Preparation of g-C3N4/ZnMoCdS hybrid heterojunction catalyst with outstanding nitrogen photofixation performance under visible light via hydrothermal post-treatment, Dalton Trans. 45 (2016) 3497–3505, https://doi.org/10.1039/C5DT04901F.

[89] S. Hu, Y. Li, F. Li, Z. Fan, H. Ma, W. Li, X. Kang, Construction of g-C_3N_4/$Zn_{0.11}Sn_{0.12}Cd_{0.88}S_{1.12}$ hybrid heterojunction catalyst with outstanding nitrogen photofixation performance induced by sulfur vacancies, ACS Sustain. Chem. Eng. 4 (2016) 2269–2278, https://doi.org/10.1021/acssuschemeng.5b01742.

[90] R.D. Milton, S. Abdellaoui, N. Khadka, D.R. Dean, D. Leech, L.C. Seefeldt, S.D. Minteer, Nitrogenase bioelectrocatalysis: heterogeneous ammonia and hydrogen production by MoFe protein, Energy Environ. Sci. 9 (2016) 2550–2554, https://doi.org/10.1039/C6EE01432A.

[91] C.-C. Chang, S.-R. Li, H.-L. Chou, Y.-C. Lee, S. Patil, Y.-S. Lin, C.-C. Chang, Y.J. Chang, D.-Y. Wang, Photoactive earth-abundant iron pyrite catalysts for electrocatalytic nitrogen reduction reaction, Small. 15 (2019) 1904723, https://doi.org/10.1002/smll.201904723.

[92] E. Mateo-Marti, S. Galvez-Martinez, C. Gil-Lozano, M.-P. Zorzano, Pyrite-induced uv-photocatalytic abiotic nitrogen fixation: implications for early atmospheres and Life, Sci. Rep. 9 (2019) 15311, https://doi.org/10.1038/s41598-019-51784-8.

[93] M. Lashgari, P. Zeinalkhani, Ammonia photosynthesis under ambient conditions using an efficient nanostructured FeS_2/CNT solar-energy-material with water feedstock and nitrogen gas, Nano Energy. 48 (2018) 361–368, https://doi.org/10.1016/j.nanoen.2018.03.079.

[94] W. Zhang, P. Xing, J. Zhang, L. Chen, J. Yang, X. Hu, L. Zhao, Y. Wu, Y. He, Facile preparation of novel nickel sulfide modified $KNbO_3$ heterojunction composite and its enhanced performance in photocatalytic nitrogen fixation, J. Colloid Interface Sci. 590 (2021) 548–560.

[95] L. Chen, X. Dai, X. Li, J. Wang, H. Chen, X. Hu, H. Lin, Y. He, Y. Wu, M. Fan, A novel $Bi_2S_3/KTa_{0.75}Nb_{0.25}O_3$ nanocomposite with high efficiency for photocatalytic and piezocatalytic N_2 fixation, J. Mater. Chem. A. 9 (22) (2021) 13344–13354.

[96] X. Dai, L. Chen, Z. Li, X. Li, J. Wang, X. Hu, L. Zhao, Y. Jia, S.-X. Sun, Y. Wu, CuS/$KTa_{0.75}Nb_{0.25}O_3$ nanocomposite utilizing solar and mechanical energy for catalytic N_2 fixation, J. Colloid Interface Sci. 603 (2021) 220–232.

[97] L.u. Chen, J. Wang, X. Li, J. Zhang, C. Zhao, X. Hu, H. Lin, L. Zhao, Y. Wu, Y. He, Facile preparation of $Ag_2S/KTa_{0.5}Nb_{0.5}O_3$ heterojunction for enhanced performance in catalytic nitrogen fixation via photocatalysis and piezo-photocatalysis, Green Energy Environ. (2022).

[98] S. Tu, Y. Guo, Y. Zhang, C. Hu, T. Zhang, T. Ma, H. Huang, Piezocatalysis and piezo-photocatalysis: catalysts classification and modification strategy, reaction mechanism, and practical application, Adv. Funct. Mater. 30 (2020) 2005158.

[99] P. Xing, P. Chen, Z. Chen, X. Hu, H. Lin, Y. Wu, L. Zhao, Y. He, Novel ternary MoS2/C-ZnO composite with efficient performance in photocatalytic NH3 synthesis under simulated sunlight, ACS Sustain. Chem. Eng. 6 (11) (2018) 14866–14879.

[100] C. Yang, Y. Zhu, J. Liu, Y. Qin, H. Wang, H. Liu, Y. Chen, Z. Zhang, W. Hu, Defect engineering for electrochemical nitrogen reduction reaction to ammonia, Nano Energy 77 (2020), https://doi.org/10.1016/j.nanoen.2020.105126 105126.

[101] X. Chen, Y. Guo, X. Du, Y. Zeng, J. Chu, C. Gong, J. Huang, C. Fan, X. Wang, J. Xiong, Atomic structure modification for electrochemical nitrogen reduction to ammonia, Adv. Energy Mater. 10 (2020) 1903172, https://doi.org/10.1002/aenm.201903172.

[102] S. Chen, X. Liu, J. Xiong, L. Mi, X.-Z. Song, Y. Li, Defect and interface engineering in metal sulfide catalysts for the electrocatalytic nitrogen reduction reaction: a review, J. Mater. Chem. A. 10 (2022) 6927–6949, https://doi.org/10.1039/D2TA00070A.

[103] Y. Liu, H. Wang, X. Yuan, Y. Wu, H. Wang, Y.Z. Tan, J.W. Chew, Roles of sulfur-edge sites, metal-edge sites, terrace sites, and defects in metal sulfides for photocatalysis, Chem Catal. 1 (2021) 44–68, https://doi.org/10.1016/j.checat.2021.01.002.

[104] C. Ma, N. Zhai, B. Liu, S. Yan, Defected MoS_2: an efficient electrochemical nitrogen reduction catalyst under mild conditions, Electrochimica Acta. 370 (2021), https://doi.org/10.1016/j.electacta.2020.137695 137695.

[105] L. Ma, W. Kong, M. Liu, Z. Jin, Y. Han, J. Sun, J. Liu, Y. Xu, J. Li, Sulfur defect-rich WS2−x nanosheet electrocatalysts for N_2 reduction, Sci. China Mater. 64 (8) (2021) 1910–1918.

[106] C. Li, R. Xu, S. Ma, Y. Xie, K. Qu, H. Bao, W. Cai, Z. Yang, Sulfur vacancies in ultrathin cobalt sulfide nanoflowers enable boosted electrocatalytic activity of nitrogen reduction reaction, Chem. Eng. J. 415 (2021), https://doi.org/10.1016/j.cej.2021.129018 129018.

[107] L. Zhao, Y. Xiong, X. Wang, R. Zhao, X. Chi, Y. Zhou, H. Wang, Z. Yang, Y.-M. Yan, Shearing sulfur edges of VS_2 electrocatalyst enhances its nitrogen reduction performance, Small 18 (11) (2022) 2106939.

[108] D. Guo, S. Wang, J. Xu, W. Zheng, D. Wang, Defect and interface engineering for electrochemical nitrogen reduction reaction under ambient conditions, J. Energy Chem. 65 (2022) 448–468, https://doi.org/10.1016/j.jechem.2021.06.012.

[109] L. Niu, D. Wang, K. Xu, W. Hao, L. An, Z. Kang, Z. Sun, Tuning the performance of nitrogen reduction reaction by balancing the reactivity of N_2 and the desorption of NH_3, Nano Res. 14 (2021) 4093–4099, https://doi.org/10.1007/s12274-021-3348-5.

[110] H.-B. Wang, J.-Q. Wang, R. Zhang, C.-Q. Cheng, K.-W. Qiu, Y. Yang, J. Mao, H. Liu, M. Du, C.-K. Dong, X.-W. Du, Bionic design of a Mo(IV)-Doped FeS_2 catalyst for electroreduction of dinitrogen to ammonia, ACS Catal. 10 (2020) 4914–4921, https://doi.org/10.1021/acscatal.0c00271.

[111] J. Zhang, X. Tian, M. Liu, H. Guo, J. Zhou, Q. Fang, Z. Liu, Q. Wu, J. Lou, Cobalt-modulated molybdenum-dinitrogen interaction in MoS_2 for catalyzing ammonia synthesis, J. Am. Chem. Soc. 141 (2019) 19269–19275, https://doi.org/10.1021/jacs.9b02501.

[112] K. Chu, J. Wang, Y. Liu, Q. Li, Y. Guo, Mo-doped SnS_2 with enriched S-vacancies for highly efficient electrocatalytic N_2 reduction: the critical role of the Mo–Sn–Sn trimer, J. Mater. Chem. A. 8 (2020) 7117–7124, https://doi.org/10.1039/D0TA01688H.

[113] J. Gao, L. Li, J. Tan, H. Sun, B. Li, J.C. Idrobo, C.V. Singh, T.-M. Lu, N. Koratkar, Vertically oriented arrays of ReS_2 nanosheets for electrochemical energy storage and electrocatalysis, Nano Lett. 16 (2016) 3780–3787, https://doi.org/10.1021/acs.nanolett.6b01180.

[114] F. Qi, X. Wang, B. Zheng, Y. Chen, B. Yu, J. Zhou, J. He, P. Li, W. Zhang, Y. Li, Self-assembled chrysanthemum-like microspheres constructed by few-layer ReSe2 nanosheets as a highly efficient and stable electrocatalyst for hydrogen evolution reaction, Electrochimica Acta. 224 (2017) 593–599, https://doi.org/10.1016/j.electacta.2016.12.097.

[115] F. Lai, N. Chen, X. Ye, G. He, W. Zong, K.B. Holt, B. Pan, I.P. Parkin, T. Liu, R. Chen, Refining energy levels in ReS_2 nanosheets by low-valent transition-metal doping for dual-boosted electrochemical ammonia/hydrogen production, Adv. Funct. Mater. 30 (2020) 1907376, https://doi.org/10.1002/adfm.201907376.

[116] Y. Kong, Y. Li, B. Yang, Z. Li, Y. Yao, J. Lu, L. Lei, Z. Wen, M. Shao, Y. Hou, Boron and nitrogen co-doped porous carbon nanofibers as metal-free electrocatalysts for highly efficient ammonia electrosynthesis, J. Mater. Chem. A. 7 (2019) 26272–26278, https://doi.org/10.1039/C9TA06076F.

[117] P. Song, H. Wang, L. Kang, B. Ran, H. Song, R. Wang, Electrochemical nitrogen reduction to ammonia at ambient conditions on nitrogen and phosphorus co-doped porous carbon, Chem. Commun. 55 (2019) 687–690, https://doi.org/10.1039/C8CC09256G.

[118] L.-P. Yuan, Z.-Y. Wu, W.-J. Jiang, T. Tang, S. Niu, J.-S. Hu, Phosphorus-doping activates carbon nanotubes for efficient electroreduction of nitrogen to ammonia, Nano Res. 13 (2020) 1376–1382, https://doi.org/10.1007/s12274-020-2637-8.

[119] L. Zeng, S. Chen, J. van der Zalm, X. Li, A. Chen, Sulfur vacancy-rich N-doped MoS_2 nanoflowers for highly boosting electrocatalytic N_2 fixation to NH_3 under ambient conditions, Chem. Commun. 55 (2019) 7386–7389, https://doi.org/10.1039/C9CC02607J.

[120] H. Fei, T. Guo, Y. Xin, L. Wang, R. Liu, D. Wang, F. Liu, Z. Wu, Sulfur vacancy engineering of MoS_2 via phosphorus incorporation for improved electrocatalytic N_2 reduction to NH_3, Appl. Catal. B Environ. 300 (2022), https://doi.org/10.1016/j.apcatb.2021.120733 120733.

[121] Q. Li, Y. Guo, Y. Tian, W. Liu, K. Chu, Activating VS2 basal planes for enhanced NRR electrocatalysis: the synergistic role of S-vacancies and B dopants, J. Mater. Chem. A. 8 (2020) 16195–16202, https://doi.org/10.1039/D0TA05282E.

[122] J. Liang, S. Ma, J. Li, Y. Wang, J. Wu, Q. Zhang, Z. Liu, Z. Yang, K. Qu, W. Cai, Boosting the acidic electrocatalytic nitrogen reduction performance of MoS2 by strain engineering, J. Mater. Chem. A. 8 (2020) 10426–10432, https://doi.org/10.1039/D0TA03622F.

[123] Y.P. Zhu, C. Guo, Y. Zheng, S.-Z. Qiao, Surface and interface engineering of noble-metal-free electrocatalysts for efficient energy conversion processes, Acc. Chem. Res. 50 (2017) 915–923, https://doi.org/10.1021/acs.accounts.6b00635.

[124] Y. Guo, Z. Yao, B.J.J. Timmer, X. Sheng, L. Fan, Y. Li, F. Zhang, L. Sun, Boosting nitrogen reduction reaction by bio-inspired FeMoS containing hybrid electrocatalyst over a wide pH range, Nano Energy 62 (2019) 282–288, https://doi.org/10.1016/j.nanoen.2019.05.051.

[125] M. Yang, Z. Jin, C. Wang, X. Cao, X. Wang, H. Ma, H. Pang, L. Tan, G. Yang, Fe Foam-supported FeS_2–MoS_2 electrocatalyst for N_2 reduction under ambient conditions, ACS Appl. Mater. Interfaces 13 (2021) 55040–55050, https://doi.org/10.1021/acsami.1c16284.

[126] G. Yang, L. Zhao, G. Huang, Z. Liu, S. Yu, K. Wang, S. Yuan, Q. Sun, X. Li, N. Li, Electrochemical fixation of nitrogen by promoting N_2 adsorption and N-N triple bond cleavage on the CoS_2/MoS_2 nanocomposite, ACS Appl. Mater. Interfaces 13 (2021) 21474–21481, https://doi.org/10.1021/acsami.1c04458.

[127] P.-Y. Liu, K. Shi, W.-Z. Chen, R. Gao, Z.-L. Liu, H. Hao, Y.-Q. Wang, Enhanced electrocatalytic nitrogen reduction reaction performance by interfacial engineering of MOF-based sulfides $FeNi_2S_4$/NiS hetero-interface, Appl. Catal. B Environ. 287 (2021), https://doi.org/10.1016/j.apcatb.2021.119956 119956.

[128] D. Zhang, Y. Liu, B. Mao, H. Li, T. Jiang, D. Zhang, W. Dong, W. Shi, Double-phase heterostructure within Fe-doped Cu2–xS quantum dots with boosted electrocatalytic nitrogen reduction, ACS Sustain. Chem. Eng. 9 (2021) 2844–2853, https://doi.org/10.1021/acssuschemeng.0c08708.

[129] M. Yuan, Y. Bai, J. Zhang, T. Zhao, S. Li, H. He, Z. Liu, Z. Wang, G. Zhang, Work function regulation of nitrogen-doped carbon nanotubes triggered by metal nanoparticles for efficient electrocatalytic nitrogen fixation, J. Mater. Chem. A. 8 (2020) 26066–26074, https://doi.org/10.1039/D0TA08914A.

[130] H.Y.F. Sim, J.R.T. Chen, C.S.L. Koh, H.K. Lee, X. Han, G.C. Phan-Quang, J.Y. Pang, C.L. Lay, S. Pedireddy, I.Y. Phang, E.K.L. Yeow, X.Y. Ling, ZIF-induced d-band modification in a bimetallic nanocatalyst: achieving over 44 % efficiency in the ambient nitrogen reduction reaction, Angew. Chem. 132 (2020) 17145–17151, https://doi.org/10.1002/ange.202006071.

[131] A. Biswas, S. Nandi, N. Kamboj, J. Pan, A. Bhowmik, R.S. Dey, Alteration of electronic band structure via a metal-semiconductor interfacial effect enables high faradaic efficiency for electrochemical nitrogen fixation, ACS Nano 15 (2021) 20364–20376, https://doi.org/10.1021/acsnano.1c08652.

[132] Y. Zhou, X. Yu, X. Wang, C. Chen, S. Wang, J. Zhang, MoS_2 nanosheets supported gold nanoparticles for electrochemical nitrogen fixation at various pH value, Electrochimica Acta 317 (2019) 34–41, https://doi.org/10.1016/j.electacta.2019.05.111.

[133] B.H.R. Suryanto, D. Wang, L.M. Azofra, M. Harb, L. Cavallo, R. Jalili, D.R.G. Mitchell, M. Chatti, D.R. MacFarlane, MoS_2 polymorphic engineering enhances selectivity in the electrochemical reduction of nitrogen to ammonia, ACS Energy Lett. 4 (2019) 430–435, https://doi.org/10.1021/acsenergylett.8b02257.

[134] T. Yang, T.T. Song, J. Zhou, S. Wang, D. Chi, L. Shen, M. Yang, Y.P. Feng, High-throughput screening of transition metal single atom catalysts anchored on molybdenum disulfide for nitrogen fixation, Nano Energy 68 (2020), https://doi.org/10.1016/j.nanoen.2019.104304 104304.

[135] X.-F. Yang, A. Wang, B. Qiao, J. Li, J. Liu, T. Zhang, Single-atom catalysts: a new frontier in heterogeneous catalysis, Acc. Chem. Res. 46 (2013) 1740–1748, https://doi.org/10.1021/ar300361m.

[136] J. Li, S. Chen, F. Quan, G. Zhan, F. Jia, Z. Ai, L. Zhang, Accelerated dinitrogen electroreduction to ammonia via interfacial polarization triggered by single-atom protrusions, Chem 6 (2020) 885–901, https://doi.org/10.1016/j.chempr.2020.01.013.

[137] K. Chu, Y. Liu, Y. Li, Y. Guo, Y. Tian, Two-dimensional (2D)/2D interface engineering of a MoS_2/C_3N_4 heterostructure for promoted electrocatalytic nitrogen fixation, ACS Appl. Mater. Interfaces. 12 (2020) 7081–7090, https://doi.org/10.1021/acsami.9b18263.

[138] P. Chen, N. Zhang, S. Wang, T. Zhou, Y. Tong, C. Ao, W. Yan, L. Zhang, W. Chu, C. Wu, Y. Xie, Interfacial engineering of cobalt sulfide/graphene hybrids for highly efficient ammonia electrosynthesis, Proc. Natl. Acad. Sci. 116 (2019) 6635–6640, https://doi.org/10.1073/pnas.1817881116.

[139] S.L. Foster, S.I.P. Bakovic, R.D. Duda, S. Maheshwari, R.D. Milton, S.D. Minteer, M.J. Janik, J.N. Renner, L.F. Greenlee, Catalysts for nitrogen reduction to ammonia, Nat. Catal. 1 (2018) 490–500, https://doi.org/10.1038/s41929-018-0092-7.

[140] D. Zhang, H. Zhao, X. Wu, Y. Deng, Z. Wang, Y. Han, H. Li, Y. Shi, X. Chen, S. Li, J. Lai, B. Huang, L. Wang, Multi-site electrocatalysts boost pH-universal nitrogen reduction by high-entropy alloys, Adv. Funct. Mater. 31 (2021) 2006939, https://doi.org/10.1002/adfm.202006939.

[141] K. Lu, F. Xia, B. Li, Y. Liu, I.B.A. Razak, S. Gao, J. Kaelin, D.E. Brown, Y. Cheng, Synergistic multisites $Fe_2Mo_6S_8$ electrocatalysts for ambient nitrogen conversion to ammonia, ACS Nano (2021), https://doi.org/10.1021/acsnano.1c07771.

[142] Y. Fu, T. Li, G. Zhou, J. Guo, Y. Ao, Y. Hu, J. Shen, L. Liu, X. Wu, Dual-metal-driven selective pathway of nitrogen reduction in orderly atomic-hybridized Re_2MnS_6 ultrathin nanosheets, Nano Lett. 20 (2020) 4960–4967, https://doi.org/10.1021/acs.nanolett.0c01037.

[143] X. Wu, Z. Wang, Y. Han, D. Zhang, M. Wang, H. Li, H. Zhao, Y. Pan, J. Lai, L. Wang, Chemically coupled NiCoS/C nanocages as efficient electrocatalysts for nitrogen reduction reactions, J. Mater. Chem. A. 8 (2020) 543–547, https://doi.org/10.1039/C9TA10142J.